



HAL
open science

Onset of the supercontinent cycle: Evidence for multiple oceanic arc accretion events in the Paleoproterozoic Sefwi Greenstone Belt of the West African Craton

H.B. Mcfarlane, N. Thébaud, L.A. Parra-Avila, R. Armit, C. Spencer, J. Ganne, L. Aillères, L. Baratoux, P.G. Betts, M.W. Jessell

► To cite this version:

H.B. Mcfarlane, N. Thébaud, L.A. Parra-Avila, R. Armit, C. Spencer, et al.. Onset of the supercontinent cycle: Evidence for multiple oceanic arc accretion events in the Paleoproterozoic Sefwi Greenstone Belt of the West African Craton. *Precambrian Research*, 2019, 335, pp.105450 -. 10.1016/j.precamres.2019.105450 . hal-03488724

HAL Id: hal-03488724

<https://hal.science/hal-03488724>

Submitted on 20 Jul 2022

HAL is a multi-disciplinary open access archive for the deposit and dissemination of scientific research documents, whether they are published or not. The documents may come from teaching and research institutions in France or abroad, or from public or private research centers.

L'archive ouverte pluridisciplinaire **HAL**, est destinée au dépôt et à la diffusion de documents scientifiques de niveau recherche, publiés ou non, émanant des établissements d'enseignement et de recherche français ou étrangers, des laboratoires publics ou privés.



Distributed under a Creative Commons Attribution - NonCommercial 4.0 International License

Onset of the supercontinent cycle: evidence for multiple oceanic arc accretion events in the Paleoproterozoic Sefwi Greenstone Belt of the West African Craton

Authors:

McFarlane, H. B.^{1,2,3}, Thébaud, N.³, Parra-Avilla, L.A.^{3,4}, Armit, R.¹, Spencer, C.⁵, Ganne, J.², Aillères, L.¹, Baratoux, L.^{2,6}, Betts, P. G.¹, and Jessell, M. W.^{2,3}

Affiliations:

¹School of Earth, Atmosphere and Environment, Monash University, 9 Rainforest Walk, Clayton, VIC 3800, Australia,

²Géosciences Environnement Toulouse, Observatoire Midi-Pyrénées, IRD, 14 ave E. Belin, Toulouse 31400 France

³ Centre for Exploration Targeting, School of Earth Sciences, The University of Western Australia, 35 Stirling Hwy, Crawley, WA 6009 Australia helen.mcfarlane@uwa.edu.au

⁴ Australian Research Council Centre of Excellence for Core to Crust Fluid Systems, School of Earth Sciences, The University of Western Australia, 35 Stirling Highway, Crawley, WA 6009, Australia

⁵ Earth Dynamics Research Group, The Institute of Geoscience Research, Department of Applied Geology, Curtin University, Perth, Australia

⁶ IFAN, Cheikh Anta Diop, Dakar, Senegal

Abstract

Greenstone belts preserved in the West African Craton (2300–2070 Ma) provide key information for understanding the petrogenetic processes and geodynamic setting for juvenile crust formation during a nascent Paleoproterozoic plate tectonic regime. New geochemical and isotopic data are presented for the magmatic suites exposed in Sefwi Greenstone Belt, SW Ghana. We define five distinct plutonic suites, with extrusive equivalents, including: 1) two generations of high SiO₂, Na₂O-rich tonalite-trondhjemite-granodiorite (TTG) granitoids; 2) calc-alkaline, LILE-enriched diorites; 3) tholeiitic pyroxenite, gabbro and layered mafic intrusives; 4) high-K quartz monzonites; and, 5) incompatible element rich, two-mica granites and muscovite leucogranites. Trace element patterns of most magmatic suites display negative Nb-Ta, P and Ti anomalies and weakly positive Pb anomalies, suggesting magma genesis in a subduction setting with minor crustal contamination/assimilation. Complementary zircon U-Pb and Lu-Hf data indicate contemporaneous emplacement of diorites ($\epsilon Hf_{(t)} = +2.5$ to $+5.4$) and low-HREE TTGs ($\epsilon Hf_{(t)} = +4.3$ to $+7.6$) between ca. 2159 and 2153 Ma, derived from contrasting sources, namely the partial melting of the metasomatised mantle wedge and high-pressure partial melting of low-K mafic sources, respectively. High-HREE TTGs are attributed to the shallow, partial melting of mafic material. The emplacement of high-K quartz monzonites ($\epsilon Hf_{(t)} = +2.5$ to $+5.2$) at ca. 2135 Ma reveals mixing of mantle-derived magmas and remelting of existing TTGs in the crustal pile. Consistently positive $\epsilon Hf_{(t)}$ values indicate predominantly radiogenic, though heterogeneous, magma sources during crustal growth, derived from precursory material extracted from the depleted mantle and an older crustal component with a minimum age of 2650 Ma. Magmatogenesis of two-mica granites and leucogranites (ca. 2092 and 2081 Ma) is interpreted to be the product of crustal anatexis during an oceanic arc-arc collisional event, with a proposed suture parallel to the NW margin of the Sefwi Belt. We hypothesise that the

formation and accretion of the West African Craton reflects the rapid amalgamation of individual oceanic arc terranes, providing potential insight into the transitional plate tectonic regime that may have characterised the Earth between 3000 and 2000 Ma.

Key words: Paleoproterozoic; subduction-collision; juvenile magmatism; Zircon Lu-Hf; West African Craton

1 Introduction

The Archean and Proterozoic rock record reveals temporal changes in the mechanisms and processes associated with crustal growth and its preservation. These changes reflect the secular cooling of the Earth, the differentiation of the Earth's crust and evolving plate dynamics (e.g. Davies, 2001; Hawkesworth & Kemp, 2006a; Herzberg, *et al.*, 2010). Some crustal growth models indicate that more than 50% of the cumulative volume of continental crust had formed by 3.0 Ga (Belousova, *et al.*, 2010; Cawood, *et al.*, 2013; Dhuime, *et al.*, 2012; Taylor & McLennan, 1985) with continuous additions hypothesised from the early Earth through to the present day. However, major changes are recorded in the continental rock record between 3.0 and 2.5 Ga, including the geochemical evolution of volcanic and plutonic rocks (Keller & Schoene, 2012; Laurent, *et al.*, 2014; Moyen & Martin, 2012), the diversification and secular evolution of the metamorphic record (Brown, 2006; Brown, 2007a) and changes in orogenic strain patterns, crustal architecture and rheology (Cagnard, *et al.*, 2011; Chardon, *et al.*, 2009; Rey & Houseman, 2006). Such secular evolution signals significant changes in global geodynamics, often interpreted as the commencement of some form of plate tectonics (Condie & Aster, 2010; Condie & O'Neill, 2010; Keller & Schoene, 2012; Sizova, *et al.*, 2010; Windley, 1984). Indeed the onset of plate tectonics is likely responsible for the transition from net crustal growth to major lithospheric recycling and reworking as part of the Wilson cycle, with the destruction or consumption of tectonic plates in subduction zones (e.g. Cawood, *et al.*, 2013; Condie, 2018; Dhuime, *et al.*, 2012).

A number of datasets within the geological record illustrate distinct clusters of magmatic and tectonic activity during the evolution of the early Earth. Episodic crustal growth is suggested by peaks in the juvenile crust record at 2.7, 1.9 and 1.2 Ga (Cawood, *et al.*, 2009; Condie, 1995; Condie, 1998; Condie, 2013); the orogenic record displays discrete events at ca. 3.80–

3.50, 2.90–2.60, 1.90–1.60, and 1.20–0.90 Ga (e.g. Zhao, *et al.*, 2002), whilst the U-Pb detrital zircon ages define peak clusters at 2.70, 2.50, 2.01, 1.84, 1.65, 1.15 and 0.60 Ga (Condie, *et al.*, 2005; Condie, *et al.*, 2011; Puetz, *et al.*, 2017). These peaks often coincide with supercontinent formation (e.g. Condie & Aster, 2010; Nance, *et al.*, 1988; Rogers & Santosh, 2004), however, they all represent periods during which conditions were favourable for preservation of the crust (Hawkesworth, *et al.*, 2009; 2010), depending on the rock type used to investigate the global U-Pb age distribution (Puetz, *et al.*, 2018). Falling between these maxima, cratonic domains of the West African-Sao Luis Craton and Guiana Shield record a period of significant juvenile crustal growth during the early Paleoproterozoic (2.25–2.07 Ga) and represent a large proportion of the extant geologic record of this time period (Spencer, *et al.*, 2018). Furthermore, these cratonic domains are some of the youngest cratonic provinces on Earth (Abouchami, *et al.*, 1990; Boher, *et al.*, 1992; Gasquet, *et al.*, 2003; Gruau, *et al.*, 1985; Klein, *et al.*, 2005; Taylor, *et al.*, 1992). Production and preservation of juvenile crust is attributed to the Eburnean–Trans-Amazonian Orogen (Abouchami, *et al.*, 1990; Boher, *et al.*, 1992; Bonhomme, 1962), marking the onset of the 2.1–1.8 Ga period of global orogenesis that heralded the rise of the Paleoproterozoic supercontinent Nuna (or Columbia) (Betts, *et al.*, 2016; Rogers & Santosh, 2002; Zhao, *et al.*, 2002). Juvenile Paleoproterozoic rocks of the southern portion of the West African Craton comprise narrow, elongate greenstone belts, voluminous granite-gneiss domains and wide sedimentary basins. The Paleoproterozoic province shares lithological and architectural similarities with Archean granite-greenstone provinces such as the Superior Province of the Canadian Shield (Card, 1990; Condie, 2015; Condie & Benn, 2006; Daigneault, *et al.*, 2002; Percival, *et al.*, 1994), the Kaapvaal Craton and the Limpopo Belt (de Wit, *et al.*, 1992; Poujol, *et al.*, 2003; Zeh, *et al.*, 2009; Zeh, *et al.*, 2013), and the Kola and Karelian provinces of the Baltic Shield (Sorjonen-Ward & Luukkonen, 2005, and references therein).

This study reports new whole-rock major and trace element geochemical data for twenty-nine igneous samples and ion microprobe (SHRIMP II) U-Pb and LA-MC-ICP-MS Lu-Hf zircon data for four samples. The selected samples are representative of the major magmatic suites exposed in the Sefwi Greenstone Belt, Kumasi and Sunyani metasedimentary domains of southwest Ghana. The aim of this study is to examine the magmatic suites emplaced in southern Ghana, complementing existing stratigraphic and sedimentary studies (e.g. Davis, *et al.*, 1994; Perrouty, *et al.*, 2012) and further contribute to the understanding of the crustal evolution of an archetypal Paleoproterozoic greenstone belt. This investigation provides insight into the crustal architecture and assembly of the West African Craton (WAC), with implications for other Paleoproterozoic orogens (e.g. Klein, *et al.*, 2005; Théveniaut, *et al.*, 2006), mineral exploration (Goldfarb, *et al.*, 2017; Groves, *et al.*, 1998) and the dynamics of the nascent Paleoproterozoic plate tectonic regime. We consider the potential significance of these findings within the context of the understudied transition from stagnant lid to modern plate tectonics between 3 Ga and 2 Ga (Condie, 2018).

2 Paleoproterozoic geology of West Africa

The West African Craton (WAC) encompasses the northern Reguibat Rise and the sub-Saharan Leo-Man Rise (Abouchami, *et al.*, 1990; Potrel, *et al.*, 1998; Rollinson, 2016). They are separated by the overlying Mesoproterozoic-Palaeozoic Taoudeni Basin. The 3600–2600 Ma Kénéma-Man Domain is juxtaposed to the Paleoproterozoic Baoulé-Mossi Domain along the Sassandra Shear Zone (Fig. 1) (Attoh & Ekwueme, 1997; Bessoles, 1977). The Baoulé-Mossi domain is dominated by rocks of the Birimian Supergroup (2300 – 2125 Ma), forming linear, N- to NE-trending volcanic greenstone belts and broad volcano-sedimentary domains, often bounded by craton-scale shear zones and separated by vast granite-gneiss terranes (Hirdes, *et al.*, 1996; Junner, 1940; Leube, *et al.*, 1990). Volcanic belts are commonly

unconformably overlain by fluvio-deltaic sequences of the Tarkwa Group and equivalents (2107–2097 Ma) (e.g. Baratoux, *et al.*, 2011; Perrouty, *et al.*, 2012; Pigois, *et al.*, 2003; Zitzmann, *et al.*, 1997). Paleoproterozoic orogenesis in West Africa is often divided into two phases, the Eoeburnean (~2300–2150 Ma), also referred to as Tangaeen or Eburnean I, (Allibone, *et al.*, 2002; de Kock, *et al.*, 2011; de Kock, *et al.*, 2012; Perrouty, *et al.*, 2012; Tshibubudze, *et al.*, 2009) and the Eburnean phase (2130–2070 Ma) (Bonhomme, 1962; Feybesse, *et al.*, 2006; Oberthür, *et al.*, 1998; Pouclet, *et al.*, 2006). Voluminous granitoid input, crustal thickening and high grade metamorphism are attributed to the Eoeburnean, whilst the Eburnean is characterised by dominantly transcurrent tectonics (de Kock, *et al.*, 2012; Feybesse, *et al.*, 2006; Vidal, *et al.*, 2009).

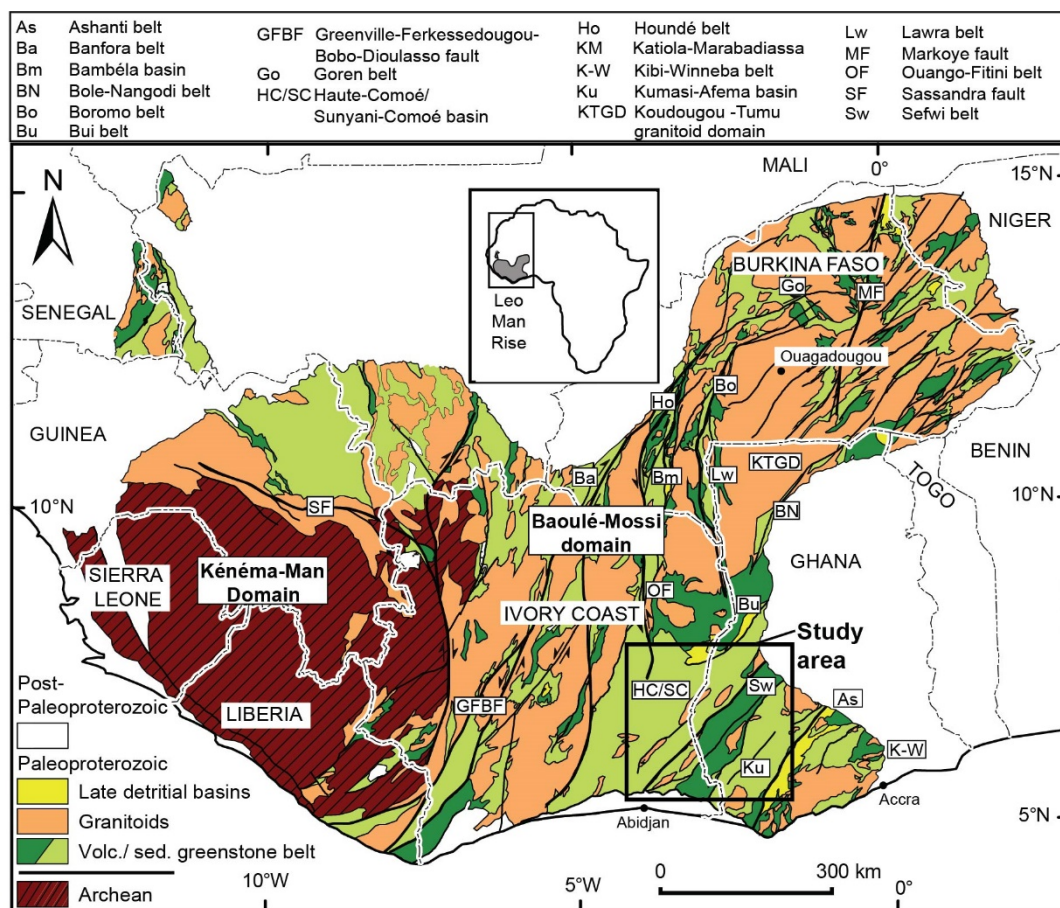


Fig. 1. Simplified map of the West African Craton showing the Archean Kénéma-Man Domain and the Paleoproterozoic Baoulé-Mossi Domain, comprising volcanic greenstone

belts (dark green), meta-sedimentary basins (light green) and large granitoid domains (orange). Yellow areas represent late fluvio-deltaic sequences of the Tarkwa Group (modified after BRGM SIGAfrique map, Milési, et al., 2004).

Volcanic rocks of the Birimian Supergroup range in composition from basalt to rhyolite, displaying tholeiitic to calc-alkaline affinities (e.g. Baratoux, et al., 2011; Hirdes, *et al.*, 1993; Senyah, *et al.*, 2016; Sylvester & Attoh, 1992), with subordinate intercalations of volcanoclastic or immature sedimentary rocks. Volcano-sedimentary domains comprise deformed sequences of greywacke, shale, argillite, volcanoclastic rocks (pyroclastic and epiclastic) and calc-alkaline volcanic sequences (Hirdes, et al., 1993; Leube, et al., 1990). The volcanic and volcano-sedimentary rocks are intruded by voluminous, compositionally diverse plutonic rocks, including diorite, TTG, high-K granite and leucogranite suites.

Mafic to intermediate volcanism occurred across the craton between 2300 and 2180 Ma (e.g. Agyei Duodu, et al., 2009; Delor, *et al.*, 1995; Feybesse, et al., 2006; Hirdes & Davis, 1998; Lompo, 2009), approximately coeval with the earliest pulse of TTG magmatism (de Kock, et al., 2011; Gueye, *et al.*, 2007; Hirdes, et al., 1992; Oberthür, et al., 1998; Siegfried, *et al.*, 2009). The most significant volumes of syn- to late-tectonic granitoid intrusions, however, were emplaced near-continuously between 2150 and 2100 Ma, yet preserved no clear lateral age gradients (Agyei Duodu, et al., 2009; Doumbia, *et al.*, 1998; Egal, *et al.*, 2002; Gasquet, et al., 2003; Hirdes, et al., 1992; Hirdes, et al., 1996; Oberthür, et al., 1998; Tapsoba, *et al.*, 2013; Tshibubudze, *et al.*, 2013). More evolved and differentiated felsic granitoids and lavas emplaced between 2100 and 2070 Ma are largely restricted to southern Mali, the Kédougou-Kéniéba Inlier and along the Archean-Paleoproterozoic contact (Egal, et al., 2002; Gueye, et al., 2007; Hirdes & Davis, 2002; Parra-Avila, *et al.*, 2017), with a significant, but localised population documented in southern Ghana along the northwest margin of the Sefwi Belt (Agyei Duodu, et al., 2009; Hirdes, et al., 1992; Hirdes, et al., 2007). Isotopic studies of

2300–2070 Ma magmatic suites yield radiogenic ϵNd values of +1.2 to +4.3, corresponding to Nd model ages of 2500 to 2200 Ma, short crustal residence times and limited Archean influence (Abouchami, et al., 1990; Boher, et al., 1992; Gasquet, et al., 2003; Pawlig, *et al.*, 2006; Peucat, *et al.*, 2005). Nd and Hf-model ages reported in a small number of studies from far south-eastern Ghana and in the western portion of the Baoulé-Mossi domain, however, suggest a greater Archean crustal influence or reworking of older Archean crust (Parra-Avila, *et al.*, 2016; Petersson, et al., 2017; Petersson, et al., 2016; Taylor, et al., 1992).

Many authors liken the evolution from bimodal tholeiitic volcanism to calc-alkaline volcanism to the development of a modern-day oceanic island arc setting (Ama Salah, *et al.*, 1996; Arndt, *et al.*, 1997; Baratoux, et al., 2011; Béziat, *et al.*, 2000; Dampare, *et al.*, 2008; Soumaila, *et al.*, 2008; Sylvester & Attah, 1992). Other authors attribute the wide-spread tholeiitic basaltic volcanism and associated plutonic activity to the plume-related formation of an oceanic plateau (Abouchami, et al., 1990; Augustin & Gaboury, 2017; Boher, et al., 1992; Lompo, 2009). Alternatively, authors have invoked intra-cratonic rifting leading to the opening of oceans and the formation of accretionary systems (Leube, et al., 1990) or a transtensional back-arc basin setting (Vidal & Alric, 1994).

The crustal architecture and structural evolution of the West African Craton are attributed to lateral shortening during the Eoeburnean and Eburnean tectonic events (e.g. Bonhomme, 1962; Eisenlohr & Hirdes, 1992; Feybesse, et al., 2006). Eoeburnean deformation is characterised by thrust-related tectonism, unit stacking and high-grade metamorphism attributed to crustal thickening (Allibone, et al., 2002; Block, *et al.*, 2015; Block, *et al.*, 2016b; Feybesse, et al., 2006; Galipp, *et al.*, 2003; Ganne, *et al.*, 2012; John, *et al.*, 1999; Milési, *et al.*, 1992). Alternatively, some authors propose that the early crustal architecture was characterised by dome and keel geometries, attributed to the diapiric uprising of granitoid bodies (Delor, et al., 1995; Lompo, 2010; Vidal, *et al.*, 1996; Vidal, et al., 2009). The widely

recognised second phase of the Eburnean Orogeny (ca. 2110–2070 Ma) is characterised by transcurrent tectonism and retrograde greenschist facies metamorphism (Allibone, et al., 2002; Feybesse, et al., 2006; Jessell, *et al.*, 2012; Pouclet, et al., 2006). Locally migmatitic, polydeformed gneissic terranes are interpreted as an older basement (>2150 Ma) upon which the Birimian volcano-sedimentary rocks were deposited (e.g. de Kock, et al., 2012; Hein, 2010; Perrouty, et al., 2012), or alternatively, as higher-grade equivalents of supracrustal sequences (Block, et al., 2015; Block, et al., 2016b; Eisenlohr & Hirdes, 1992; Hirdes, et al., 2007). Discrepancies in the geochemical, geochronological, isotopic evolution and tectono-thermal histories between terranes in the West African Craton have been used as evidence of suturing of independent cratonic fragments and collision orogenesis within the craton, (Block, et al., 2016b; Parra-Avila, 2015; Parra-Avila, et al., 2017).

3 Geology of southern Ghana

The crustal architecture of southern Ghana and southeast Ivory Coast is defined by four parallel northeast-striking, volcanic greenstone belts, the Kibi-Winneba, Ashanti, Sefwi and Bui belts (from southeast to northwest), separated by the Akyem, Kumasi-Afema and Sunyani-Comoé volcano-sedimentary basins (Agyei Duodu, et al., 2009; Hirdes, et al., 1993; Jessell, et al., 2012) (Fig. 2). The Birimian stratigraphy of southern Ghana, as defined by Perrouty, et al. (2012) for the adjacent Ashanti Belt, comprises metavolcanics and minor metasedimentary sequences of the lower Sefwi Group, dominated by tholeiitic to calc-alkaline basalt, andesite and rhyolite sequences. Geochemical analyses of derivative basalt and basaltic andesite rocks exhibit characteristics of subduction-related magmatism, such as pronounced negative Nb-Ta, Hf and Ti anomalies (Senyah, et al., 2016). Rhyolitic volcanic sequences dated in the Sefwi Belt in both Ghana and the Ivory Coast indicate volcanism was active between ca. 2189 and 2166 Ma, coeval with the emplacement of tonalite and granodiorite plutons between ca. 2163 and 2179 Ma (Hirdes, et al., 1992; Hirdes, et al., 2007).

The overlying Kumasi Group (2154 – 2125 Ma) is predominantly made of phyllites and volcanoclastic rocks, with syn-depositional andesitic volcanism dated in the Kumasi-Afema Domain at 2142 ± 24 Ma (Adadey, et al., 2009). Detrital, fluvio-deltaic sedimentary rocks of the Tarkwa Group deposited unconformably over the Sefwi Group volcanic rocks in the Ashanti belt between 2107 and 2097 Ma (Perrouy, et al., 2012; Pigois, et al., 2003).

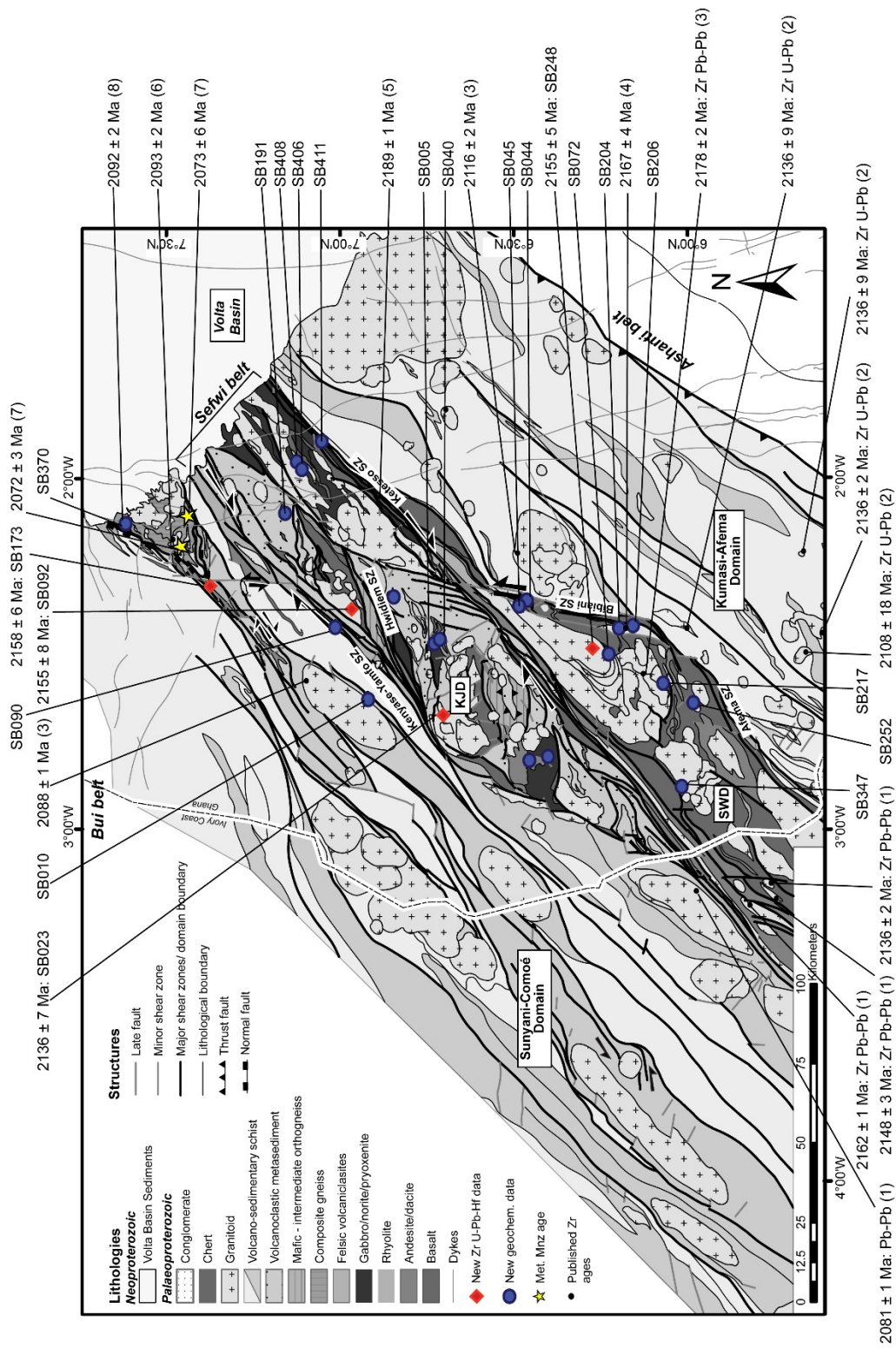


Fig. 2: Litho-structural map of the study area showing the location of samples discussed in this study and existing published geochronological data, modified after McFarlane, et al. (2019). CD = Chiraa Domain; HD = Hwidiem Domain; KJD = Kukuom-Juaboso Domain; SWD = Sefwi-Wiwaso Domain; SZ = shear zone. Zircon age: (1) Hirdes, et al. (2007); (2) Adadey, et al. (2009); (3) Hirdes, et al. (1992); (4): Petersson, et al. (2017); (5) (Cawood, et al., 2013); Hirdes and Davis (1998); (6): Petersson, et al. (2016); (7): (McFarlane, 2018); (8): Agyei Duodu, et al. (2009).

This study focuses on the Sefwi Greenstone Belt and the volcano-sedimentary Sunyani-Comoé Domain which are bounded by the northeast-striking Sefwi Shear System (Jessell, et al., 2012) including the Kenyase-Yamfo, Ketesso and Kumasi-Afema shear zones (Fig. 2). Results of the geochemical and geochronological analysis presented in this study are used to better understand the magmatic evolution of the study area, intended to complement the extensive stratigraphic studies and established stratigraphic column compiled for the neighbouring Kumasi metasedimentary domain and the Ashanti Greenstone Belt (Agyei Duodu, et al., 2009; Davis, et al., 1994; Oberthür, et al., 1998; Perrouty, et al., 2012) rather than redefining previously established stratigraphic column for the Ashanti Belt, southeast of the Sefwi Belt (Perrouty, et al., 2012).

4 Sampling and analytical methods

This study relies on a multidisciplinary approach that combines field based mapping, petrography, igneous and isotopic geochemistry and geochronology. Such an integrated approach allows for a contextual discussion on the igneous and associated geodynamic evolution of the Sefwi Belt. Detailed techniques applied in the course of this study are presented in the supplementary materials (Supplementary Information (SI) 1). The use of in-situ isotopic analysis of zircon, including both U-Pb and Lu-Hf systematics yield both the crystallisation age and the timing of extraction of the source material from the mantle (Hawkesworth & Kemp, 2006b; Patchett, *et al.*, 2004). This is a well-established method used to understand crustal evolution, crustal architecture and the geodynamic setting of crustal formation (!!! INVALID CITATION !!!).

Twenty-nine (29) fresh samples representative of the dominant lithological units, including 19 plutonic samples ranging from pyroxenite plutons to sodic granitoids to granites, and 10 basaltic to rhyolitic volcanic and volcanoclastic rock samples. These were collected from

throughout the Sefwi Greenstone Belt and the Sunyani-Comoé Domain for petrological and geochemical analysis. The locations of the samples are shown in Fig. 2, with extended petrological and lithological distribution descriptions presented in the supplementary information (SI2). Existing geochronological data, including methodology, for southern Ghana is summarised in the supplementary information (SI3 –Table SI3.1). Coordinates of samples presented in this study are given in tables SI3.1 and SI4.1.

Analytical procedures for the acquisition of whole rock major and trace element geochemistry, as well SHRIMP zircon U-Pb analysis and LA-MC-ICP-MS zircon Lu-Hf analysis are provided in the supplementary information (SI1). Reported U-Pb ages are based on accepted values (95% confidence). Samples were rejected if they showed a discordance below -3% or above +10%. The full list of conditions used for the reduction of raw SHRIMP data and removal of any analyses displaying disturbed or altered U-Pb systematics are included in SI1

5 Results

5.1 Lithological and petrological descriptions

5.1.1 Granitoids

In order to simplify the presentation and the description of the lithologies sampled in this study, analysed granitoid samples have been grouped into three main lithotypes, based on petrological composition and geochemical analysis, including: i) tonalite, trondhjemite and granodiorite (TTG); ii) quartz diorite and diorite; and iii) granite and quartz monzonite.

Within the study area, there are two series of plagioclase-rich tonalite, trondhjemite and granodiorite plutons. The first group comprises large, composite, medium- to coarse-grained, leucocratic trondhjemite and tonalite plutons that contain biotite as the main ferromagnesian

mineral with subordinate to rare hornblende (Figs. 3a and 3b) and rare interstitial microcline. The second group comprises smaller, elliptical to elongate, leucocratic to mesocratic granodiorite and trondhjemite plutons that are emplaced towards the south of the Sefwi Belt and often contain small, round, mafic enclaves. Quartz diorite and diorite plutons are medium- to coarse-grained and contain abundant hornblende phenocrysts and interlocking, subhedral to euhedral

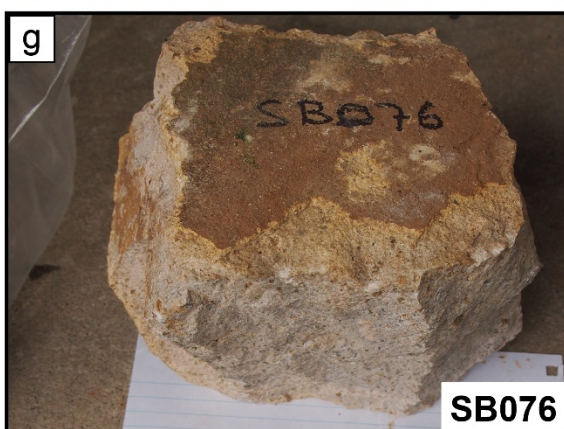
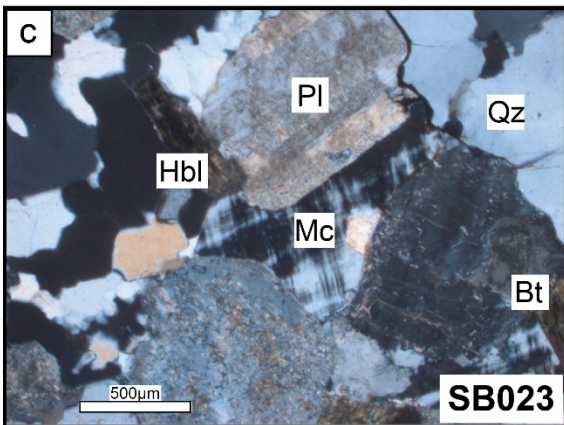


Fig. 3. Selected samples of investigated plutonic and volcanic suites: a) Medium-grained foliated biotite-hornblende trondhjemite; b) Outcrop of trondhjemite in Sefwi-Wiawso domain with a mafic enclave containing retrograde chlorite and actinolite; c) Petrographic assemblage of potassic biotite-hornblende quartz monzonite with euhedral plagioclase displaying sericite alteration, interstitial microcline (Mc) and fine biotite and hornblende crystals; d) Coarse-grained to pegmatitic biotite-muscovite granite in metatectic paragneiss; e) Typical metabasalt outcrop with chlorite-actinolite foliation; f) Hand sample of pyroxenite from the Bechem Granitoid Domain, containing clinopyroxene, minor orthopyroxene, both largely replaced by hornblende and quartz and minor plagioclase; g) Quartz-microcline-plagioclase-phyric rhyolite; h) Hornblende and plagioclase-phyric dyke cross cutting folded amphibole-garnet para-amphibolite in the Kukuom-Juaboso domain.

plagioclase often strongly altered by sericite, and minor quartz. Clinopyroxene phenocrysts often display extensive replacement rims of secondary hornblende and quartz.

Potassic granitoid samples are grouped together for comparative purposes, yet display two distinct petrological assemblages. Potassium-rich quartz monzonite plutons (Fig. 3c) occur as large (>20 km), irregular, weakly deformed composite plutons, predominantly restricted to within the Kukuom-Juaboso and Bechem Granitoid domains within the Sefwi Belt (Fig. 2). Granite samples from the Chiraa Domain are variably deformed, medium grained, irregular intrusions within high-grade metasedimentary rocks (Fig. 3d), comprising quartz, perthitic microcline and plagioclase, often displaying a metamorphic foliation defined by aligned biotite \pm muscovite. Muscovite-dominant, megacrystic white-grey leucogranite plutons (>50 km) intrude the Sunyani-Comoé Domain, elongate parallel to the NE strike of the major crustal architecture.

5.1.2 Volcanic rocks

Volcanic rocks analysed in this study range from basaltic to rhyolitic in composition, which have undergone varying degrees of low-grade metamorphism and alteration, overprinting

primary mineral assemblages. Basalt and basaltic andesite rocks contain magmatic and/or metamorphic hornblende (Fig. 3e), with foliations defined by aligned hornblende in higher grade samples, or chlorite, actinolite and calcite in lower grade samples. Field observations reveal a strong spatial association between mafic extrusive and intrusive sequences, and are therefore described together. Mafic intrusive suites include small, elongate pyroxenite and gabbro plutons exposed in central parts of the belt including the Bechem Granitoid and Kukuom-Juaboso domains and the Hwidiem Shear Zone (Fig. 2). Relative timing of their emplacement remains unclear due to lack of observable lithological contacts. The melanocratic, coarse-grained to megacrystic, equigranular plutons (Fig. 3f) comprise orthopyroxene, clinopyroxene, hornblende and plagioclase, depending on lithology and/or the presence of magmatic layering. Pyroxenes are often extensively replaced by secondary hornblende and quartz, with some outcrops containing abundant, centimetric plagioclase-rich veins that display secondary sericite alteration.

Intermediate to felsic volcanic and volcanoclastic units are found throughout the field area, often intercalated with or cross cutting sedimentary sequences. Deformed dacitic volcanoclastic rocks contain plagioclase and quartz phenocrysts and exhibit chlorite-muscovite foliations with rare preservation of foliation aligned biotite porphyroblasts. Replacement of primary plagioclase by epidote, albite and sericite is commonly observed. A number of quartz-phyric pink rhyolite outcrops are documented, observed stratigraphically overlying garnet-hornblende paragneisses in the Kukuom-Juaboso domain (Fig. 3g). Late andesite dykes contain hornblende and zoned plagioclase phenocrysts, observed in the field as a cross-cutting dyke, intrude a deformed amphibole-bearing para-amphibolite (Fig. 3h). Intermediate and felsic lavas commonly display sericite alteration, including growth of fine grained white mica. Accessory minerals include titanite, allanite and hematite.

5.2 Whole rock geochemistry

Whole rock major and trace element concentrations of investigated samples are presented in the supplementary information (Table SI4.1). Key characteristics of each of the key magmatic suites are detailed below.

5.2.2 Granitoid rocks

Sampled plutonic rocks record a wide range of silica contents. Plutons in the granite and TTG groups have high silica contents of 70–76 wt% SiO₂, with the exception of the quartz monzonite sample with 68 wt% SiO₂ (Fig. 4a). Diorite and quartz diorite rocks range from 55 to 61 wt% SiO₂ (Fig. 4a) (Table SI2). High-SiO₂, plagioclase-rich granitoids are plotted on an An-Ab-Kfs normative ternary diagram (fields from Barker, 1979; O'Connor, 1965), distinguishing tonalite, trondhjemite, granodiorite and granite rocks based on normative CIPW norms, specifically normative feldspar composition. Six samples plot in the trondhjemite field, six in the tonalite field and three in the granite field (Fig. 4b).

Quartz-diorites and diorites plot along the calc-alkaline differentiation trend in the Na-K-Ca ternary diagram. The more sodic trondhjemite and tonalite samples, as well as the quartz monzonite, plot in the Archean trondhjemite field (Fig. 4c). Granite samples plot distal to both trends, indicating Ca depletion. In the Harker diagrams (Fig. 4a), the SiO₂ vs. K₂O plot shows that the trondhjemite plutons display both tholeiitic (TH) and calc-alkaline (CA) affinities, whilst quartz-diorites and diorites plot primarily in the CA series, with one sample falling in the high-potassium calc-alkaline (HKCA) series. The quartz monzonite and granite samples all plot in the HKCA series. Overall, major oxide and silica relationships in the Harker diagrams show approximately linear differentiation trends, with increasing SiO₂ associated with decreasing MgO, CaO, TiO₂ and FeO. Weaker correlation, however, is observed between Al₂O₃, Na₂O and K₂O in relation to increasing SiO₂, consistent with minor sericite alteration as observed during petrographic analysis. Geochemical analysis of plutonic

rocks displayed only minor evidence of alteration (AI vs AAAI alteration box plot), with evidence of weak silicification on two trondhjemitic samples (Large, *et al.*, 2001). Based on petrological and geochemical evidence, the samples are interpreted as largely free of influence of secondary processes such as alteration and metamorphism.

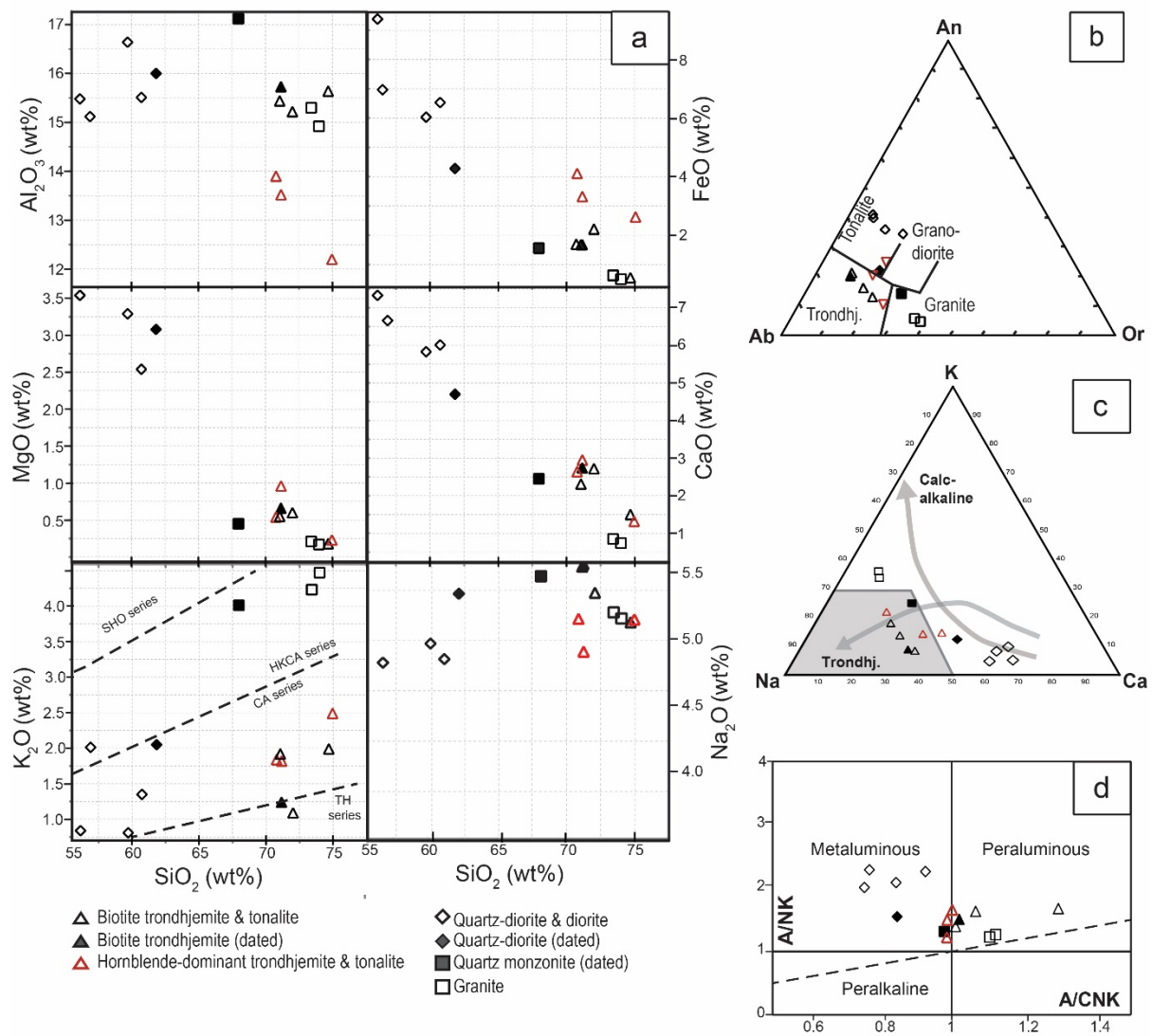


Fig. 4. Major element geochemistry of granitoids of the study area, presented in (a) Harker diagrams, (b) normative feldspar triangle with fields after ; (c) molecular Na-K-Ca ternary diagram and (d) in an A/CNK vs A/NK diagram. Symbol legend (top right) represents the lithological groups based on identification of major mineral assemblages and the

classification in the feldspar diagram, where triangles denoting tonalite and trondhjemite samples are illustrated as biotite-dominant (black) or hornblende dominant (red).

Tonalite-trondhjemite and quartz diorite plutons exhibit lower K_2O/Na_2O values (0.21 to 0.48) relative to granite and quartz monzonite plutons (0.76–1.01), however, with one sample (SB045) plotting on the tonalite-granodiorite boundary with a K_2O/Na_2O ratio of 0.56. Tonalite-trondhjemite plutons have Mg# ($100 * (\text{Molar Mg}/(\text{Mg}/\text{Fe}^{2+}))$) of 13–31, with lower values often representing hornblende-dominant granitoids, with concentration of mafic oxides ($\text{MgO} + \text{FeO}_T$) ranging between 0.73 and 4.65. By comparison granite and quartz monzonite samples have intermediate Mg# (34–37) and low mafic oxide concentrations ($\text{MgO} + \text{FeO}_T = 0.67\text{--}2.01$). Quartz diorites and diorites display a significantly higher range of Mg# values (40–59) and mafic oxide concentrations of 7.36–12.92 wt%. Tonalites and trondhjemites are slightly metaluminous to slightly peraluminous ($A/CNK = 0.99\text{--}1.07$; A/CNK: molar ratio $\text{Al}_2\text{O}_3/[\text{CaO} + \text{Na}_2\text{O} + \text{K}_2\text{O}]$ and $A/NK = 1.22\text{--}1.65$; A/NK: molar ratio $\text{Al}_2\text{O}_3/[\text{Na}_2\text{O} + \text{K}_2\text{O}]$) with one anomalously peraluminous sample ($A/CNK = 1.30$; $A/NK = 1.68$). Granites are peraluminous ($A/CNK = 1.23\text{--}1.27$; $A/NK = 1.11\text{--}1.12$) whilst the quartz monzonite is slightly metaluminous ($A/CNK = 1.31$; $A/NK = 0.98$). Quartz-diorite and diorite samples are strongly metaluminous, yielding ratios of $A/CNK = 0.76\text{--}0.93$; $A/NK = 1.55\text{--}2.26$.

Trace element geochemistry of the plutonic samples are presented in primitive mantle-normalised multi-element and chondrite-normalised rare earth element (REE) spidergrams (Fig. 5). All granitoid samples show strongly negative anomalies for high field strength elements (HFSE) (Nb-Ta, Ti). Most samples also display a positive Pb anomaly, with the exception of granite samples SB010 and SB370. Evidence of argillitic alteration, such as depletion of LILE coupled with Pb enrichment, or sericitic alteration, characterised by Cs, Rb, Ba and K and Pb, Sr, P and HREE depletion, is not observed in multi-element spidergrams (Alderton, *et al.*, 1980). Both the multi-element diagram and REE diagram reveal two distinct

tonalite-trondhjemite lithological groups, corresponding with the biotite-bearing (black triangles, Fig. 5) versus the hornblende-dominant (red triangles, Fig. 5) tonalite-trondhjemite plutons. The biotite-rich

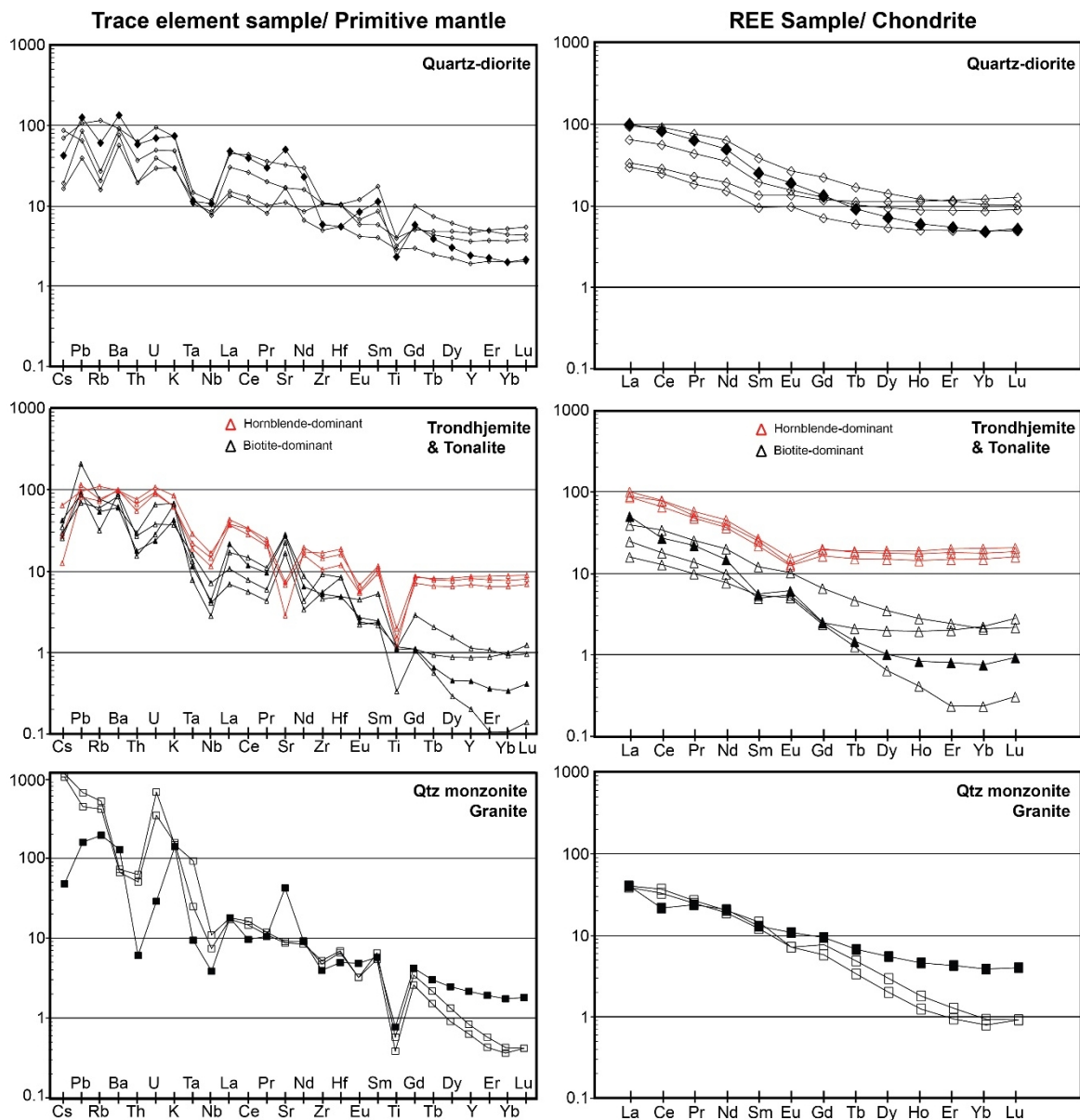


Fig. 5. Primitive-mantle normalised multi-element (McDonough, et al., 1992) and chondrite-normalised REE (McDonough & Sun, 1995) spidergrams for granitoid suites.

samples have moderate to high LREE values ($La_N = 20.67-64.97$) and low HREE-Y concentrations ($Yb_N = 0.31-2.92$) contents, resulting in a steep, more fractionated REE

spectra ($La_N/Yb_N = 10.98\text{--}66.57$). The hornblende-rich samples have flat, moderate fractionation REE spectra, corresponding with both high LREE concentration ($La_N = 111.39\text{--}129.95$) and high HREE–Y concentration ($Yb_N = 19.44\text{--}26.27$), yielding a moderately fractionated REE pattern ($La_N/Yb_N = 4.35\text{--}5.72$). Additionally, the two groups have contrasting Sr and Eu anomalies (where $Eu_N/Eu^* = 0.81\text{--}1.03$; $Eu^* = [Sm_N \times Gd_N]^{1/2}$), with the more heavily fractionated, biotite dominant group displaying strong positive Sr anomalies ($Sr = 352\text{--}600\text{ppm}$), positive Eu anomalies ($Eu_N/Eu^* = 1.14\text{--}1.62$), as well as low to moderate LILE enrichment relative to LREE ($Rb_N/La_N = 0.23\text{--}1.04$), whilst the less fractionated, hornblende dominant group displays, negative Sr anomalies ($Sr = 59\text{--}156\text{ppm}$), negative Eu anomalies ($Eu_N/Eu^* = 0.59\text{--}0.67$) and low LILE enrichment relative to LREE ($Rb_N/La_N = 0.15\text{--}0.27$), reflecting the high LREE concentrations. Quartz-diorite and diorite samples reveal intermediate REE fractionation patterns ($La_N/Yb_N = 2.86\text{--}22.90$), with moderate to high LREE contents ($La_N = 39.24\text{--}137.97$) and high HREE and Y content ($Yb_N = 6.02\text{--}15.46$). They display slightly negative to slightly positive Eu anomalies ($Eu_N/Eu^* = 0.91\text{--}1.20$), and minimal LILE enrichment relative to LREE ($Rb_N/La_N = 0.08\text{--}0.24$).

Granites samples are characterised by moderate LREE content ($La_N = 50.63\text{--}52.74$), moderate to high HREE–Y contents ($Yb_N = 1.06\text{--}1.24$) and moderate to strong REE fractionation patterns ($La_N/Yb_N = 42.45\text{--}47.95$), with the higher HREE values yielded by the quartz monzonite, indicating weaker REE fractionation ($La_N = 52.75$, $Yb_N = 5.09$, $La_N/Yb_N = 10.35$). Relative to all other samples, the granites display strong LILE enrichment ($Rb_N/La_N = 1.01\text{--}2.69$) as well as weakly negative to negative Eu anomalies ($Eu_N/Eu^* = 0.67\text{--}0.98$).

5.2.3 Volcanic rocks and mafic intrusive suites

Volcanic samples from across the study area are plotted on the TAS diagram (Le Maitre, *et al.*, 1989) displaying a range of compositions from basalt to rhyolite (Fig. 6a). All pyroxenite and gabbro samples plot in the basalt field (red circles; Fig. 6a). Nine of the ten volcanic

samples plot in the sub-alkaline field, whilst a quartz-feldspar-phyric rhyolite sample (SB076) is slightly alkaline. In the AFM diagram, most volcanic samples plot (Fig. 6b) in the calc-alkaline field, whilst a metabasalt (SB164) and one meta-dacite (SB016) and the mafic intrusive samples display tholeiitic compositions. Dacitic samples largely plot close to the calc-alkaline field boundary, indicating more Fe-rich compositions. Mafic extrusive and intrusive samples exhibit similar geochemical characteristics, including low K_2O/Na_2O (0.16–0.32), and elevated Mg# (47–73) and mafic oxide concentration ($MgO + FeO_T = 18.4–25.6$ wt %). One gabbro records an elevated K_2O/Na_2O of 0.59, likely as a product of metamorphic processes. Pyroxenite and gabbro samples are strongly metaluminous, yielding ratios of $A/CNK = 0.16–0.68$; $A/NK = 2.04–3.88$.

Basalt and basaltic andesite samples [Cr (6–1990 ppm), Ni (105–109 ppm) and V (142–256 ppm)] and mafic intrusive equivalents record elevated heavy metal concentration [Cr (133–1240 ppm), Ni (81–208 ppm), Sc (19–63 ppm), V (153–305 ppm)], reflecting a common peridotite mantle source (Green, 1980), with the high values in pyroxenite samples potentially indicative of cumulates. Basalt sample SB164 displays positive Pb and Sr anomalies, a negative Zr anomaly, and a relatively flat trace element spectra, indicating element mobility during regional metamorphism (Ague, 2017). The basalt-andesite displays weak LILE enrichment with weakly positive Ba, U and La anomalies, as well as a positive Pb anomaly. Overall the group shows very weak LILE enrichment ($Rb_N = 0.21–1.48$; $Rb_N/La_N = 0.01–0.04$) and neither sample displays a Eu anomaly ($Eu_N/Eu^* = 1.02 – 1.11$). Pyroxenite and gabbro samples display slightly negative to no Eu anomalies, and extremely low enrichment in large ion lithophile elements (LILE) ($Rb_N/La_N = 0.01–0.22$), associated with moderately negative Rb, weakly positive Ba and mixed Sr anomalies (Sr = 94–460 ppm). Both meta-basalt and basaltic andesite samples have similar REE patterns characterised by moderate LREE ($La_N = 16.88–42.19$) and HREE–Y ($Yb_N = 10.87–11.49$) contents, and low

REE fractionation ($\text{La}_N/\text{Yb}_N = 1.47 - 3.88$). Mafic intrusive suites display comparable flat to weakly fractionated REE patterns and ratios ($\text{La}_N/\text{Yb}_N = 1.25 - 4.04$). Dacites display more fractionated REE patterns, with moderate to high LREE content ($\text{La}_N = 37.55-110.97$) and moderate to high HREE–Y content ($\text{Yb}_N =$

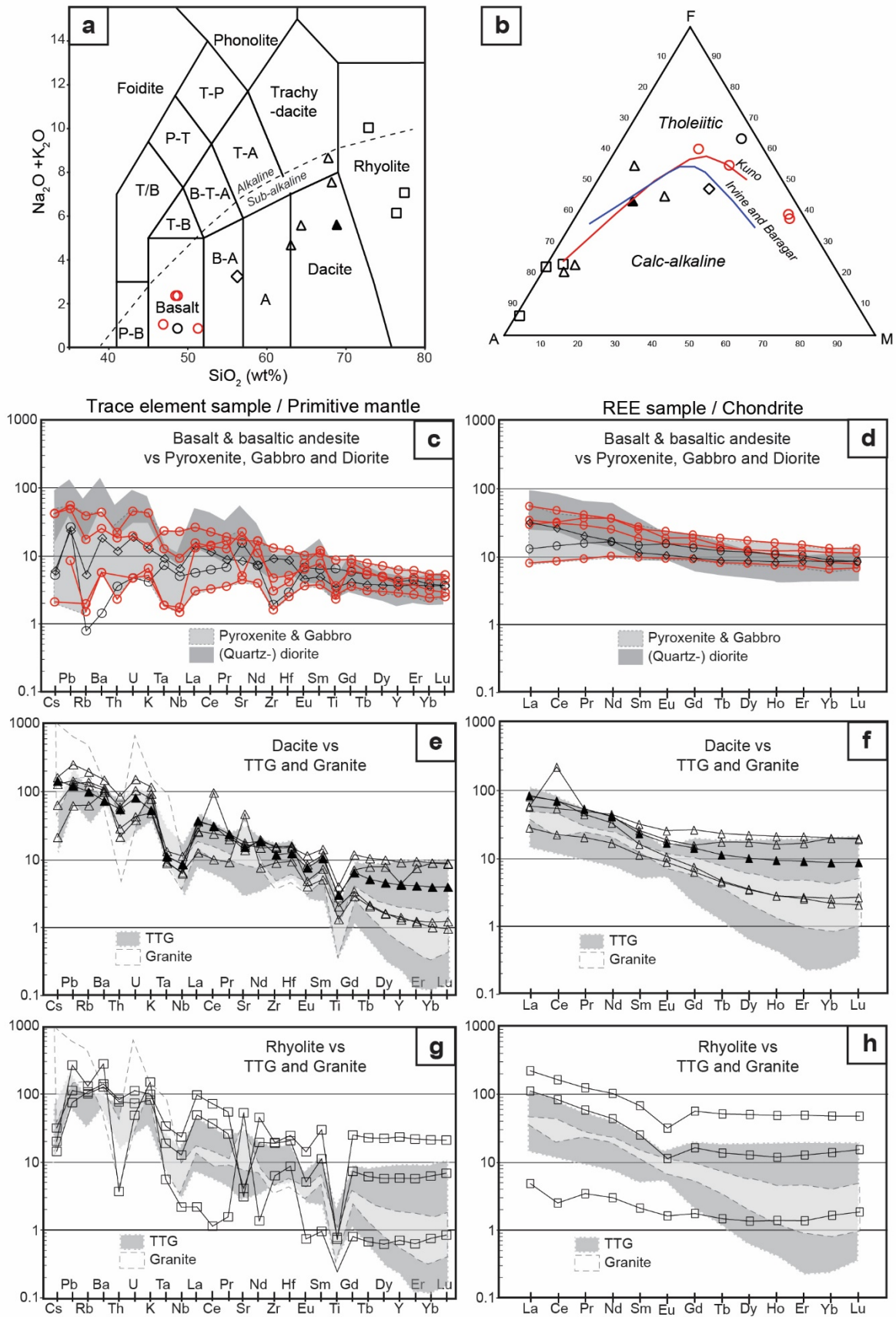


Fig. 6. Geochemistry of volcanic units (black) and mafic-ultramafic (red) plutonic suites. (a) TAS diagram (Le Maitre, et al., 1989) displaying volcanic samples from across the field area, ranging

from basalt (circle) to basaltic andesite (diamond) to dacite (triangle) and rhyolite (square), including mafic-ultramafic intrusive suits (red circles) for comparison. (P-B) Picro-basalt; (B-A) Basaltic andesite; (A) Andesite; (T-A) Trachyandesite; (B-T-A) Basaltic trachyandesite; (T-B) Trachybasalt; (T/B) Tephrite/ Basanite; (P-T) Phonotephrite; (T-P) Tephriphonolite. (b) AFM ternary diagram (Irvine & Baragar, 1971; Kuno, 1968) where A is $Na_2O = K_2O$, F is FeO_T and M is MgO. (c, e, g) Primitive-mantle normalised trace element (McDonough, et al., 1992) and (d, f, h) chondrite-normalised REE (McDonough & Sun, 1995) spidergrams plotted over range of trace element and REE compositions of major plutonic suites.

2.98 – 26.58), and $La_N/Yb_N = 2.86-30.15$. Dacites display LILE enrichment ($Rb_N = 17.34 - 53.91$; $Rb_N/La_N = 0.22-1.02$), strong negative HFSE anomalies (Nb, Ta, Ti) and no Sr anomalies, with the exception of a plagioclase-phyric dacite sample (SB464B), which shows a strong positive Sr anomaly. Foliated dacitic volcanoclastic sample SB090 shows unique trace element patterns, displaying a distinct positive Ce anomaly and negative Y anomaly. Eu anomalies in dacite samples are slightly negative to neutral ($Eu_N/Eu^* = 0.88 - 1.05$).

Rhyolitic samples display heterogeneous trace element patterns in multi-element diagrams, although each have negative Nb, Tb and Ti anomalies and negative Eu anomalies ($Eu_N/Eu^* = 0.52-0.85$). REE spectra for each of the rhyolites show similarly moderate REE fractionation patterns ($La_N/Yb_N = 2.91-7.94$), however, quartz-feldspar-phyric rhyolite sample (SB076) contrasts all other felsic lavas. It displays extreme LILE enrichment ($Rb_N = 35.22$; $Rb_N/La_N = 5.56$) with strong positive Pb, Ba, K and Sr (1090 ppm) anomalies, depletion in MREE and a weakly negative Eu anomalies ($Eu_N/Eu^* = 0.85$) and a REE pattern less than an order of magnitude greater than chondrite values ($Yb_N = 2.17$). Conversely, sample SB044 and SB244 are enriched in most incompatible elements and have negative Sr (63–83 ppm) and Eu ($Eu_N/Eu^* = 0.51-0.56$), with sample SB044 displaying extreme enrichment in both HREE–Y and LREE ($La_N = 282$; $Yb_N = 61.55$).

5.3 Zircon U-Pb and Lu-Hf analysis Geochronology

In-situ zircon SHRIMP U-Pb analyses were performed on four samples, including three plutonic samples and one volcanic sample. This was complemented by Lu-Hf isotope analysis by LA-MC-ICP-MS, both performed at Curtin University. Back-Scattered Electron (BSE) and cathodoluminescence (CL) imaging of zircons was performed on each sample prior to analysis, with CL images of representative grains presented in Figure 7. Detailed descriptions of zircon morphology, BSE and CL response can be found in supplementary information SI2.3. The results of zircon U-Pb and Lu-Hf analyses are shown in the tables SI4.2 and SI4.3 and Figures 8, 9 and 11, with results of standard Lu-Hf analysis presented in Table SI4.4. As most of the analyses yielded concordant or near-concordant results, crystallization ages are presented as weighted mean average age rather than Concordia diagrams.

5.3.1 Foliated biotite trondhjemite (sample SB248)

Twenty-six analyses were performed on twenty-five zircons displaying fine oscillatory zoning (Fig. 7a) from biotite trondhjemite sample SB248, located 5km north of Wiawso. Of the twenty accepted analyses, eighteen analyses from sample SB248 yielded a single age population and a weighted mean average $^{207}\text{Pb}/^{206}\text{Pb}$ age of 2153 ± 5 Ma (MSWD = 0.92, n=18) interpreted to be the crystallization age (Fig. 8a). One zircon grain yielded an older $^{207}\text{Pb}/^{206}\text{Pb}$ date of 2184 ± 12 Ma, representing a slightly older inherited component, however its internal morphology is indistinguishable from the zircons that yielded the magmatic crystallization age.

Nineteen Hf analyses in dated grains yielded $^{176}\text{Lu}/^{177}\text{Hf}$ of < 0.0007 , $^{176}\text{Yb}/^{177}\text{Hf}$ of < 0.02 and $^{176}\text{Hf}/^{177}\text{Hf}$ range from 0.281543 to 0.281630 ± 0.000034 – 0.000067 (2SE) (Fig. 9a).

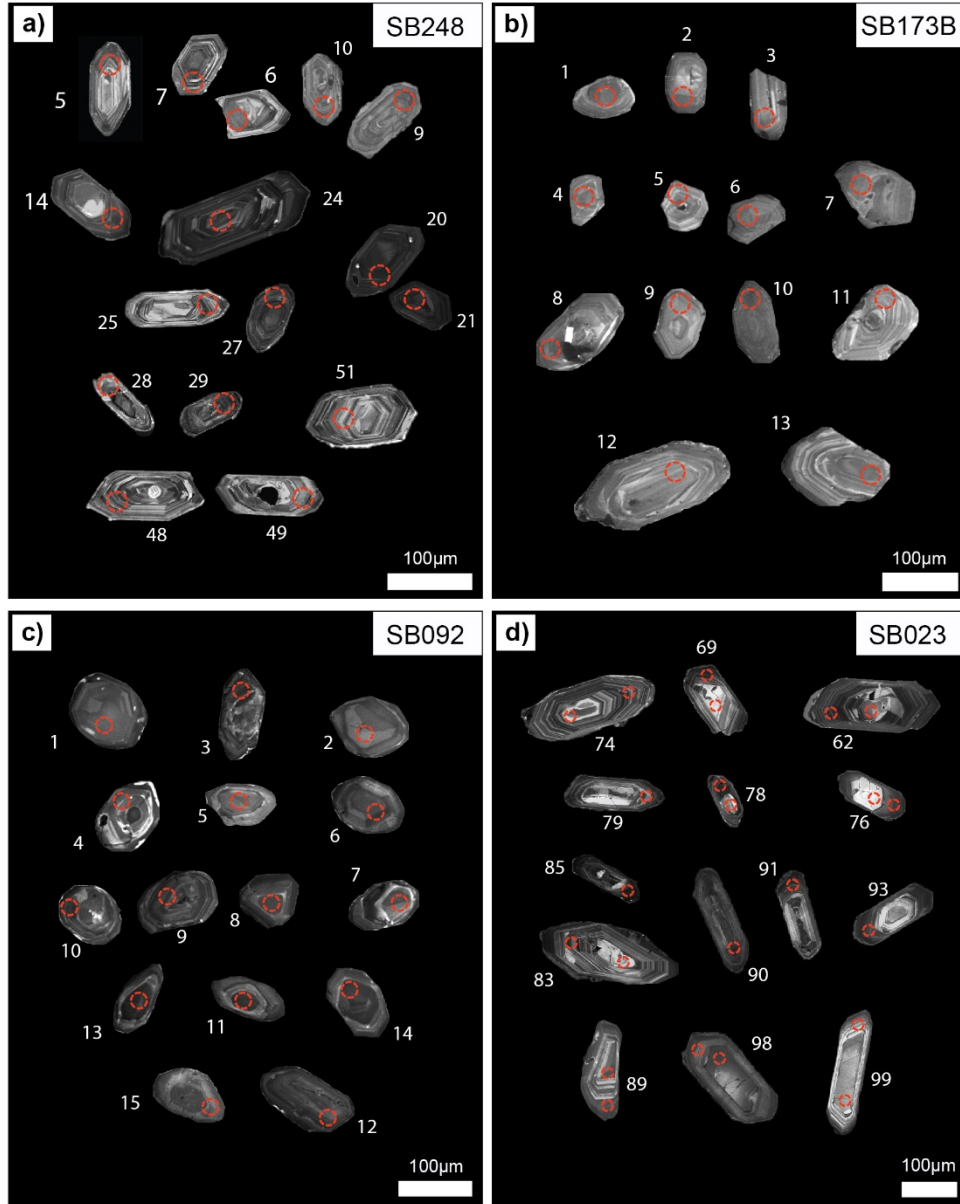


Fig. 7. Cathodoluminescence (CL) images of representative zircon grains from analysed samples showing SHRIMP spot location (red dashed circles) for both accepted and rejected analyses: a) sample SB248; b) sample Sb173b; c) sample SB092, d) sample SB023.

Individual Pb-Pb dates and initial $^{176}\text{Lu}/^{177}\text{Hf}$ ratios for each zircon reveal radiogenic $\varepsilon\text{Hf}_{(t)}$ values between +4.4 to +7.6 (mean $\varepsilon\text{Hf}_{(t)} = 6.0 \pm 0.9$), corresponding to a relatively tightly grouped range of two-stage T_{DM}^{H} model ages between 2.26 and 2.47 Ga. The inherited zircon yielded a strongly radiogenic Hf signatures of $\varepsilon\text{Hf}_{(2184\text{Ma})} = +5.6$, within range of the εHf values yielded by magmatic zircons used to calculate the crystallization age.

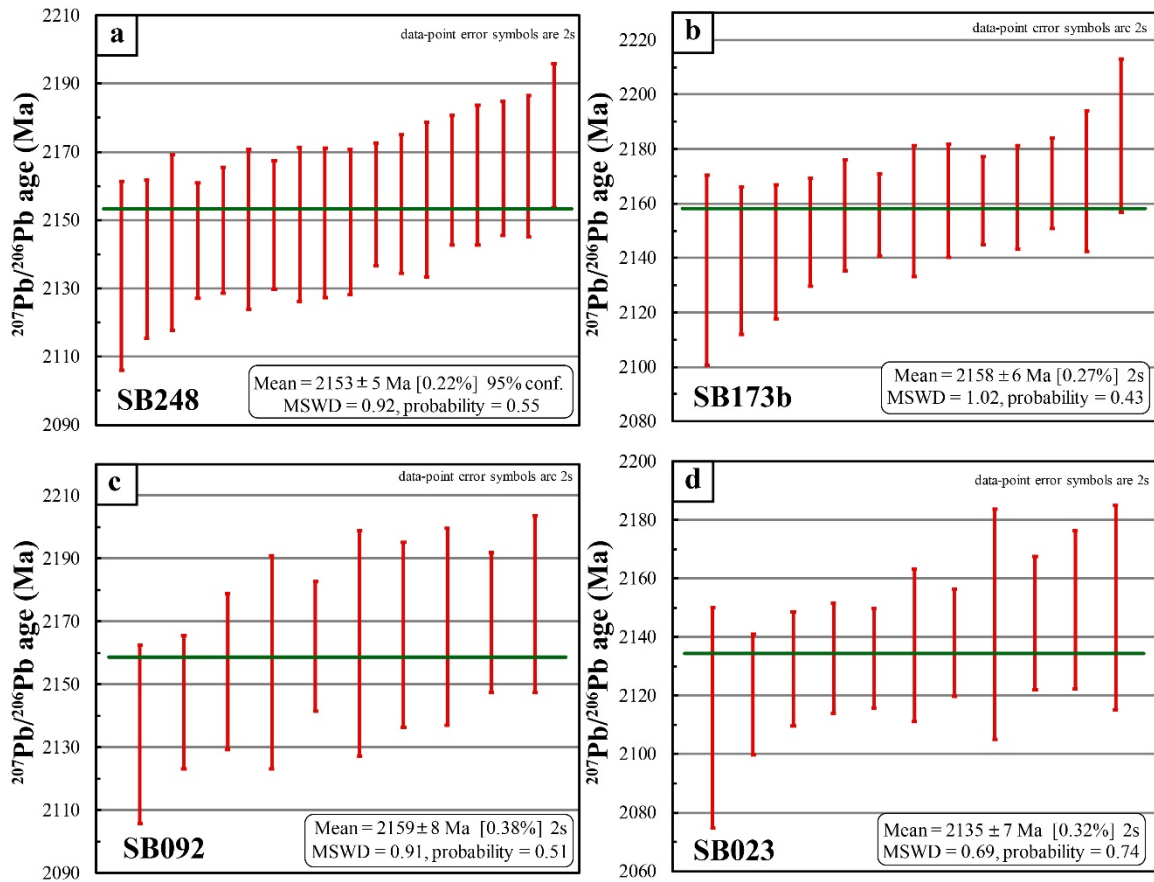


Fig. 8. Weighted average $^{207}\text{Pb}/^{206}\text{Pb}$ ages displaying SHRIMP U-Pb zircon spot data for samples (a) SB248, (b) SB173B, (c) SB092 and (d) SB023, displaying error bars of $\pm 2\sigma$ for accepted analyses. Inherited ages not shown.

5.3.2 Foliated dacitic volcanoclastite (SB173B)

Thirteen U-Pb analyses were performed on thirteen zircons from dacitic volcanoclastite sample SB173B from both oscillatory zoned and unzoned zircons (Fig. 7b), which defined a single zircon age population, which yielded a weighted average $^{207}\text{Pb}/^{206}\text{Pb}$ age of 2158 ± 6 Ma (MSWD = 1.02, $n = 13$) (Fig. 8b), interpreted as the crystallisation age of this rock. Thirteen Hf analyses were performed on dated grains yielding $^{176}\text{Lu}/^{177}\text{Hf}$ of < 0.0028 ,

$^{176}\text{Yb}/^{177}\text{Hf}$ of < 0.09 and $^{176}\text{Hf}/^{177}\text{Hf}$ range from 0.281464 to 0.281567 ($\pm 0.000043 - 0.000073$ 2SE) (Fig. 9b). A juvenile, radiogenic Hf character is indicated by a wider range of suprachondritic $\epsilon\text{Hf}(t)$ values between +1.6 and +5.7 (mean $\epsilon\text{Hf}(t) = 3.8 \pm 1.3$), corresponding to a range of T_{DM}^{H} model ages spanning from 2.40 to 2.65 Ga.

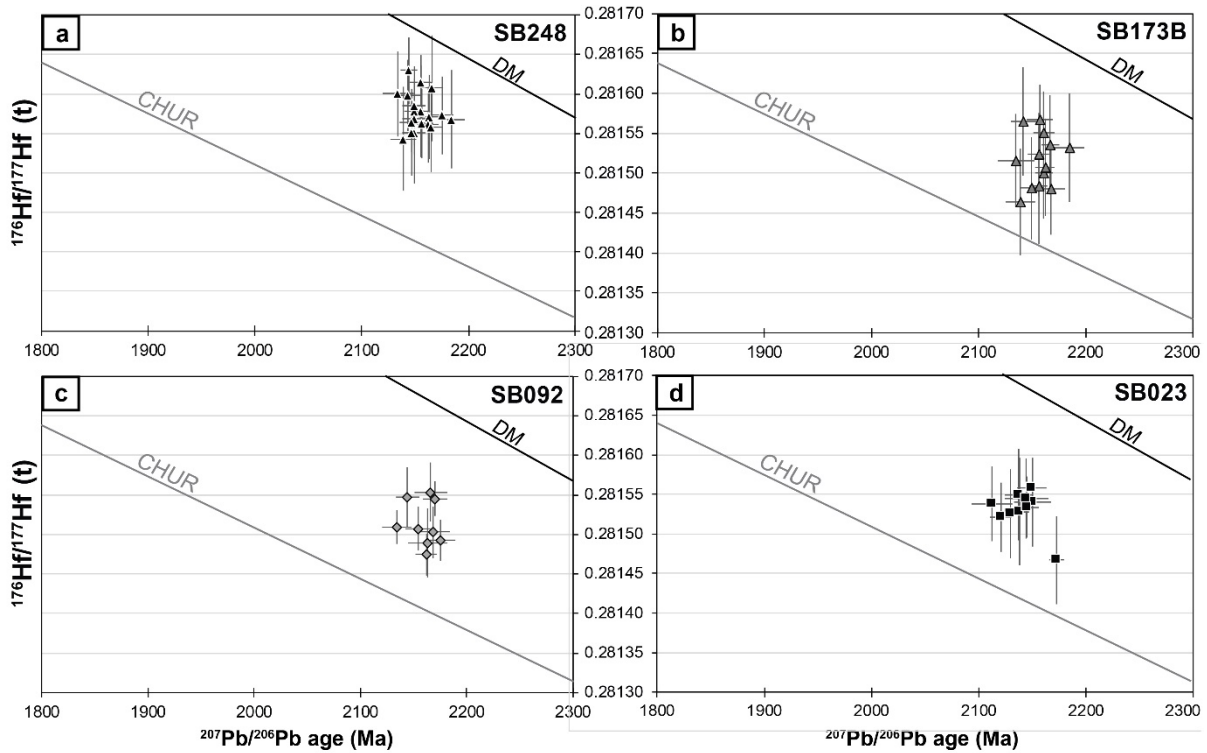


Fig. 9. Results of combined U-Pb and Lu-Hf zircon analyses for samples from the study area in southwest Ghana, presented as $^{207}\text{Pb}/^{206}\text{Pb}$ age vs $^{176}\text{Hf}/^{177}\text{Hf}(t)$, where $^{176}\text{Hf}/^{177}\text{Hf}(t)$ is the initial ratio calculated at time t , t being the $^{207}\text{Pb}/^{206}\text{Pb}$ age.

5.3.3 Hornblende quartz diorite (SB092)

Sixteen zircon U-Pb analyses were performed on sixteen zircons displaying either equant or prismatic morphology (Fig. 7c), six of which were rejected based on error. The two morphological groups yielded indistinguishable dates from ten analyses, indicating a single zircon age population that yielded a weighted average $^{207}\text{Pb}/^{206}\text{Pb}$ age of 2159 ± 8 Ma (MSWD = 0.91, $n=10$) (Fig. 8c), which is interpreted as the crystallisation age.

Nine Hf analyses on nine grains yielded $^{176}\text{Lu}/^{177}\text{Hf}$ of < 0.001 , $^{176}\text{Yb}/^{177}\text{Hf}$ of < 0.04 and $^{176}\text{Hf}/^{177}\text{Hf}$ range from 0.281475 to 0.281553 ($\pm 0.000051 - 0.000074$ 2SE) (Fig. 9c). These analyses yield a relatively radiogenic Hf signature, with suprachondritic $\epsilon\text{Hf}_{(t)}$ values ranging from +2.5 to +5.4 (mean $\epsilon\text{Hf}_{(t)} = 3.8 \pm 1.0$), which corresponds to a two-stage model age (T_{DM}^{H}) range between 2.42 and 2.61 Ga.

5.3.4 Biotite-hornblende potassic quartz monzonite (SB023)

Thirty-six analyses were performed on twenty-six grains from potassic quartz monzonite sample SB023 (Fig. 7d) in both zoned and homogeneous zircons. Multiple analyses were taken in grains displaying zonation, however, independent zones did not reveal distinct ages, or more commonly, yielded dates with higher errors. Eleven of these analyses were accepted, yielding a weighted average $^{207}\text{Pb}/^{206}\text{Pb}$ age of 2135 ± 7 Ma (MSWD = 0.69, $n = 11$), which is interpreted to be the crystallization age of the rock (Fig. 8d). Many of the zircons that displayed apparent xenocrystic cores yielded ages within error of analyses from homogeneous zircons and zircon rims, thus no discernible systematic variation could be identified.

A total of nine Hf analyses were performed on dated zircons from sample SB023, yielding $^{176}\text{Lu}/^{177}\text{Hf}$ of < 0.003 , $^{176}\text{Yb}/^{177}\text{Hf}$ between 0.01 and 0.1, and $^{176}\text{Hf}/^{177}\text{Hf}$ range from 0.281447 to 0.281558 ($\pm 0.000032 - 0.000059$ 2SE) (Fig. 9d). Analyses revealed a radiogenic Hf signature with suprachondritic $\epsilon\text{Hf}_{(t)}$ values between +2.5 and +5.2 (mean $\epsilon\text{Hf}_{(t)} = 3.9 \pm 0.8$), corresponding to a wide range of T_{DM}^{H} values, from 2.44 to 2.64 Ga.

6 Discussion and conclusions

6.1 Petrogenesis of magmatic suites

The observed major and trace element patterns of magmatic rocks may reflect several petrogenetic processes including: the source composition, magma mixing processes, fractionation crystallisation (e.g. Brown, *et al.*, 1984; Pearce, *et al.*, 1984), as well as the pressure of melt production (e.g. Defant & Kepezhinskas, 2001; Foley, *et al.*, 2002; Moyen, 2011; Moyen & Stevens, 2006a; Xiong, *et al.*, 2005). The ubiquitous negative Nb-Ta, P and Ti anomalies coupled with positive Pb anomalies and variable LILE enrichment for all samples analyses in this study, excluding one meta-gabbro and one metabasalt, are consistent with the trace element patterns of the present-day bulk continental crust (Hawkesworth & Kemp, 2006a; Hofmann, 1997; Rudnick & Gao, 2003). Such features typify arc magmas and crust formation in a subduction setting (e.g. Arculus, *et al.*, 1999), and are therefore consistent with the onset of “modern-style” subduction-related processes after 3.0 Ga (e.g. Condie & Benn, 2006; Halla, *et al.*, 2009; Laurent, *et al.*, 2014; Smithies & Champion, 2000). Magmatic rocks sampled in this study share a number of geochemical similarities with late-Archean granitoids generated within nascent subduction-related geodynamic settings, which are characterised by: (i) sodic tonalite-trondhjemite-granodiorite (TTG) granitoids derived from partial melting of hydrous metabasalts; (ii) mantle-derived, incompatible element-rich sanukitoids; (iii) biotite and two-mica granites derived from crustal sources; and, (iv) hybrid granitoids sharing petrological and geochemical similarities and sources to the first three groups (Halla, *et al.*, 2009; Laurent, *et al.*, 2014; Moyen, 2011; Moyen & Martin, 2012), suggesting somewhat comparable petrogenetic processes.

The two TTG groups are both characterised by a silicic, plagioclase-rich assemblage, distinguished from one another on the basis on the dominance of either biotite or hornblende as the primary ferromagnesian mineral. They show tholeiitic to calc-alkaline affinities and low K₂O/Na₂O ratios, with higher ratios in the hornblende-bearing TTGs reflecting slightly

higher modal proportions of potassium feldspar. Based on experimental melt compositions (Laurent, et al., 2014, and references therein), Figure 10a indicates a common low-K mafic source for both TTG groups, with the exception of two samples, with one indicating a high-K mafic source, and the second high-Al₂O₃ sample indicating remelting of pre-existing TTGs.

Two end-member models generally considered for the production of TTGs through partial melting of hydrous metabasalts are distinguished by two contrasting geodynamic settings. The first geodynamic setting for TTG production is through partial melting of a basalt underplating thickened crust (Albarède, 1998; Atherton & Petford, 1993; Bédard, 2006; de Wit, 1998; Smithies, *et al.*, 2005). The second setting is through the partial melting of a young, hot subducting slab, rather than dehydration melting (Foley, et al., 2002; Martin, 1986; Martin & Moyen, 2002; Rapp & Watson, 1995; Rapp, *et al.*, 1991). Although both groups of TTGs have low potassium values (< 3wt %), normalised LREE/HREE ratios ((La/Yb)_N = ~6.4 – 8.4)

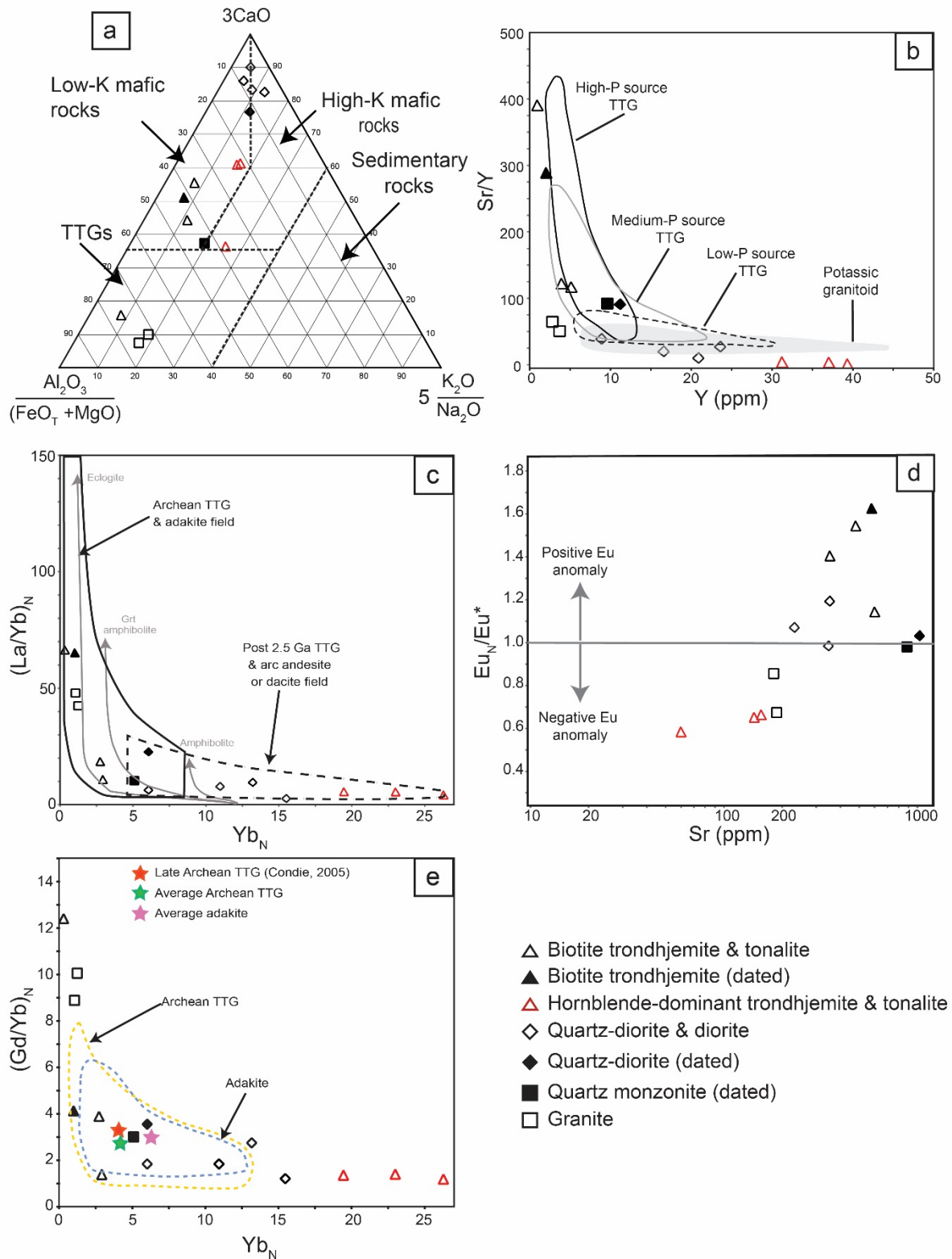


Fig. 10. a) Ternary diagram for major element of granitoid samples analysed in this study used to discriminate between potential source rocks, with fields after Laurent, et al. (2014, and references therein) based on experimental melt compositions. Binary diagrams (b-f) used

to discriminate: (b, c, d) depth of melt generation and residual phase assemblage, comparing late Archean TTGs and post-2.5Ga TTG and arc magmatism (Abati, *et al.*, 2012; Drummond & Defant, 1990; Moyen, 2011); (e) Binary diagram used to discriminate residual phase assemblage, depth and temperature of melting relative to average Archean TTGs, late Archean TTGs and adakites derived from average lower crustal material rather the downgoing slab (modified after Qian & Hermann, 2013).

indicate the hornblende-bearing granitoids show similar ratios to modern day basalt-andesite-dacite-rhyolite (BADR) arc sequences, where magma is primarily derived through metasomatism of mantle peridotite by fluids released during dehydration of the subducting slab (Martin, *et al.*, 2009). The complementary trace element patterns of the two groups of TTGs suggests a link in their magmatic history, but contrasting petrogenetic processes. REE patterns of the biotite-dominant TTG group display a strongly fractionated REE pattern, with a significant depletion in HREE–Y indicating residual garnet and/or hornblende in the magma source. High Sr/Y ratios and Y content also reflect a garnet-bearing residuum (Fig. 10b), often characterising deep melting at a convergent margin (Condie, 2008; Martin, 1993). The La_N/Yb_N vs Yb_N binary diagram (Fig. 10c) indicate high modal proportions of garnet in residuum of the garnet-eclogite source for the biotite-rich TTGs, compared to the garnet-free amphibolite indicated for the hornblende-dominant TTGs (Drummond & Defant, 1990; Laurent, *et al.*, 2014; Moyen, 2011). These high-pressure TTG melts display positive Sr and Eu anomalies (Fig. 10d), a characteristic commonly documented in slab-derived tonalite and trondhjemite melts involving subduction of young, hot oceanic crust due to the release of Sr and Eu during plagioclase breakdown at the garnet amphibolite-eclogite transition (Defant & Drummond, 1990; Drummond, *et al.*, 1996; Drummond & Defant, 1990), occurring at pressures between 1.5 and 2.0 GPa (Moyen & Stevens, 2006b; Rapp, *et al.*, 1991). Gd_N/Yb_N ratios have been used to further distinguish the residual phases and depth of melting, with

high Gd_N/Yb_N ratios (4- 15) relative to depressed Yb_N content associated with higher abundance of garnet in the residuum (Qian & Hermann, 2013). The low-pressure, hornblende dominant, high-HREE TTGs, display distinctly high Yb_N (18-26) relative to low Gd_N/Yb_N ratios (<2), consistent with high proportions of amphibole in the residuum (Qian & Hermann, 2013). As such, these magmas are considered potentially analogous to adakites generated through the partial melting of a hot, down-going slab in an oceanic environment (Defant & Drummond, 1990; Drummond, et al., 1996; Smithies, 2000). Their unusually low Mg# and high SiO_2 and elevated concentrations of Sc, V and Co would, however, suggest that evidence of interaction and assimilation with peridotite in the overlying mantle wedge has been partially obscured by subsequent amphibole fractionation (Rapp, *et al.*, 1999; Wang, *et al.*, 2006; Woodhead, *et al.*, 1993). Alternatively, these geochemical characteristics potentially record the partial melting of hydrous mafic rocks in that the base of thickened arc crust, associated with moderate to high levels of garnet in the residuum and moderate to high pressures (Qian & Hermann, 2013) for the strongly fractionated TTG suites. Accordingly, there would be no interaction with the mantle wedge, consistent with the low Mg# and Sc, V, and Co concentrations. Based on the positive Sr and Eu anomalies, potentially associated with plagioclase breakdown and depths >40 km (Martin & Moyen, 2002), we favour petrogenesis of low-HREE TTGs in the study area by partial melting of the downgoing slab, however, we acknowledge the restricted overlap with magma compositions derived from partial melting of the lower crust (Moyen, 2009; Moyen & Stevens, 2006a).

Predominantly low-K mafic sources are indicated for hornblende-bearing TTGs (Fig. 10a), however, compared to the biotite-bearing TTGs, they display lower Al_2O_3 contents, low Sr concentrations, weakly fractionated REE patterns with high HREE concentrations and slightly negative Eu anomalies. These characteristics indicate that magma production occurred within the stability field of plagioclase, indicating either plagioclase fractionation or

plagioclase as a residual phase in a garnet-free or garnet poor-residuum at pressures of <1.0 GPa (Moyen & Stevens, 2006b). These characteristics suggest a shallow, low-pressure source, such as partial melting of garnet-free basaltic crust, interpreted as analogous to the low-pressure TTG group of Moyen (2011).

Contrasting TTG magmas, the mafic intrusive and extrusive suites, as well as quartz diorite intrusions display low SiO₂ contents, high FeO_T, MgO and Mg#, and enrichment in transitional metals including Cr and Ni, thus precluding melt derivation from a crustal source. This is further highlighted by REE patterns which display less than an order of magnitude enrichment in HREE and MREE relative to primitive mantle values. Trace element patterns do, however, indicate moderate LILE and Pb enrichments for the quartz diorite suite, suggesting a crustal influence (Brown, et al., 1984; Hawkesworth & Kemp, 2006a). Based on geochemical similarities, the pyroxenite and gabbro intrusions are interpreted as potential parental magmas to mafic extrusive samples. The pyroxenite suite also potentially represents the primary magma from which the dioritic magmas evolved through fractional crystallisation during differentiation, generated thorough partial melting of an enriched mantle source. Depletion of HFSE elements, including Nb, Ta, Zr and Hf, in diorite and quartz diorite samples is typical of island arc magmas generated during dehydration melting with a rutile-bearing residuum (Foley, et al., 2002). Despite similarly low SiO₂, elevated ferromagnesian (FeO_T + MgO) content and Sr and Ba concentrations > 500 ppm, the diorite and quartz diorite samples are not considered to be analogous to the sanukitoids series frequently recorded at the Archean-Paleoproterozoic boundary, due to lower MgO concentrations, Mg# and weaker REE fractionation (Martin, et al., 2009; Martin, *et al.*, 2005; Shirey & Hanson, 1984; Stern, *et al.*, 1989).

Three samples plot in the high-K calc-alkaline field, including the biotite-hornblende quartz monzonite and two granites. The quartz monzonite sample displays a similar composition to

the high-pressure TTGs in terms of REE distribution and a positive Sr anomaly, but features a higher K_2O/Na_2O ratio, greater concentrations of Rb, Ba and K, as well as lower SiO_2 and no Eu anomaly. It may represent the mixture of magmas from a metasomatised mantle source and partial melting of pre-existing high-pressure TTG sources (Feng & Kerrich, 1992).

In contrast, the two-mica granite and the muscovite-bearing leucogranite samples, which display higher SiO_2 contents with elevated K_2O/Na_2O (0.93–1.01), reflect higher modal proportion of potassium feldspar. These granites display strongly fractionated REE patterns, substantial enrichment in LILE and negative Eu anomalies (Fig. 10d), indicating plagioclase fractionation or melt generation within the stability field of plagioclase, consistent with geochemical characteristics of S-type granites generated through partial melting of metasedimentary rocks (Clemens, 2003; Clemens & Vielzeuf, 1987). These granites are interpreted as the product of shallow partial melting during orogenesis of enriched crustal sources, including sedimentary packages, further supported by field observations (Fig. 3d), and calculated metamorphic conditions for anatectic terranes detailed by McFarlane (2018). Within the Sefwi Belt, the extremely low REE content of a sampled rhyolite (SB076) is a reflection of its petrological assemblage which contains no ferromagnesian phases, potentially sourced from a nearby crustal source.

6.2 Timing of juvenile crust formation and crustal recycling

The temporal evolution of magmatism is compatible with contemporaneous emplacement of high-pressure TTGs derived from melting of the subducting, young, hot, oceanic lithosphere, and quartz diorite melts derived from an enriched mantle source. Both TTG and diorite melt are emplaced into mafic to intermediate volcanic rocks in the Sefwi-Wiawso Domain (SW Ghana and SE Ivory Coast) that yielded crystallisation ages between ca. 2189 and 2162 Ma (Hirdes & Davis, 1998; Hirdes, et al., 2007). The dacitic volcanoclastite sample from the

Sunyani Basin yielded a zircon U-Pb crystallisation age of 2158 ± 6 Ma and displays similar trace element patterns to the low-pressure TTGs, and is therefore interpreted as an extrusive equivalent. The coeval emplacement of chemically equivalent tonalite and trondhjemite plutons and felsic volcanic rocks is consistent with previous geochemical and geochronological studies of the Sefwi Belt. For example, andesitic and rhyolitic flows and volcanoclastic rocks within the Sefwi Belt yield U-Pb and Pb-Pb zircon ages between ca. 2189 and 2164 (Hirdes & Davis, 1998; Hirdes, et al., 2007), partly contemporaneous with the emplacement of “belt-type” or “Dixcove-type” hornblende-bearing TTG granitoids into volcanic rocks of the Sefwi Belt between ca. 2179 and 2154 Ma (Hirdes, et al., 1992; Hirdes, et al., 2007; Petersson, et al., 2017). The timing of emplacement of the pyroxenite and gabbro suite, however, remains poorly understood. Samples documented in this study are consistent with pyroxenites documented in south-eastern Ivory Coast also indicating a LILE-enriched upper mantle source (Hirdes, et al., 2007). These intrusions exhibit strong geochemical affinities to the tholeiitic basalt sequences, thus likely represent the sub-volcanic equivalent to early tholeiitic basaltic magmatism in the belt.

About 20 to 25 Myrs following TTG and diorite emplacement, high-K quartz monzonites yield zircon crystallisation ages of 2136 ± 7 Ma and interpreted as the product of remelting of existing high-pressure TTGs by mantle derived magmas. Quartz monzonite magmatism in the study area coincides with the emplacement of monzonitic and arfvedsonite-bearing albite granite magmatism between ca. 2145 and 2135 Ma in the Ivorian extent of the Sefwi-Wiawso Domain (Hirdes, et al., 2007).

Two-mica and muscovite granitoids are emplaced in the Sunyani-Comoé Domain along the north-western margin between ca. 2092 and 2081 Ma (Agyei Duodu, et al., 2009; Hirdes, et al., 1992; Hirdes, et al., 2007; Petersson, et al., 2016), associated with crustal thickening and anatexis of felsic or supracrustal rocks (McFarlane, 2018; McFarlane, et al., 2019). The

muscovite granite sample (SB010) is taken from the margin of a muscovite-bearing granitoid that yielded Pb-Pb ages of 2088 ± 1 Ma (Hirdes, et al., 1992) and the two-mica granite (SB370) was sampled from the Wenchi pluton dated at 2092 ± 2 Ma (Agyei Duodu, et al., 2009), suggesting that granite magmas occur significantly later in the magmatic history of Sunyani-Comoé Domain. The original spatial relationships between the Sefwi Belt and the Sunyani-Comoé Domain is largely obscured by deformation during the Eburnean Orogeny; however, we proposed that the tectonic contacts between the two domains represents a narrow collisional front or suture, with evidence of collision between the two discrete crustal fragments, represented by southern Ghana and central Ghana/Ivory Coast, recorded by the emplacement of syn-collisional granites (Fig. 12f) between ca. 2092 and 2081 Ma, and high-P, intermediate-T metamorphism and clockwise P-T metamorphic paths (McFarlane, 2018; McFarlane, et al., 2019).

Zircons from magmatic rocks analysed in this study display consistently suprachondritic ϵ_{Hf} values with a wide vertical array between +1.6 and +7.6 at the time of zircon crystallisation reflecting a predominantly radiogenic source and juvenile nature of the newly formed crust with an older felsic crustal component. Furthermore, the juvenile Hf signature of all samples suggests that significantly older, Archean crustal material was largely absent or distal during juvenile crust production, consistent with the findings of previous studies of Paleoproterozoic rocks in the West Africa Craton that yielded positive ϵ_{Nd} between +1.2 and +4.3 (Abouchami, et al., 1990; Boher, et al., 1992; Gasquet, et al., 2003; Taylor, et al., 1992). Trondhjemitic sample SB248 with an interpreted crystallization age of 2153 ± 5 Ma shows a narrow, radiogenic vertical array with ϵ_{Hf} values between +4.3 and +7.6, representing a relatively homogeneous, largely juvenile source. The quartz diorite sample (SB092) with a crystallization age of 2159 ± 8 Ma yielded ϵ_{Hf} values between +2.5 and +5.4, indicating a more significant older crustal component, whilst a greater range of ϵ_{Hf} values was yielded

by the 2158 ± 6 Ma dacitic volcanoclastite (+1.6 to +5.7) suggesting local variation in source heterogeneity. Whilst geochemical analysis of the younger 2135 ± 7 Ma quartz monzonite displays evidence of magma mixing, its associated ϵ_{Hf} values yielded a vertical array of values between +2.5 and +5.2, revealing a larger component of older crustal material with ongoing radiogenic input. Two-stage Hf model ages for all samples range from 2650 Ma and 2260 Ma (Fig. 13). This indicates the minimum possible age for the older crustal component is approximately 2650 Ma, assuming a depleted mantle source. This minimum age does not imply, however, that the older crustal component was necessarily extracted at precisely 2650 Ma.

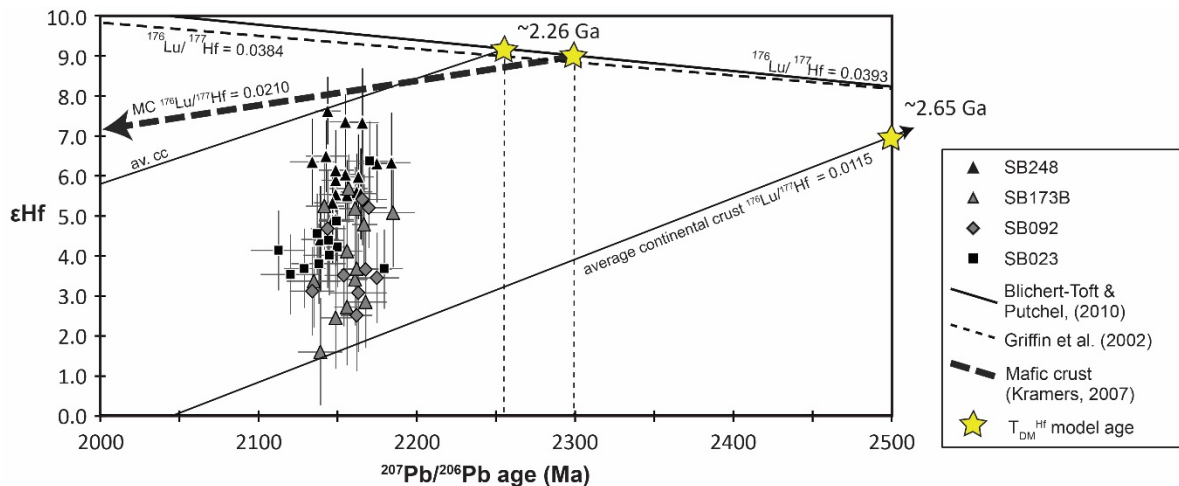


Fig. 13. ϵ_{Hf} values versus Pb-Pb age diagram for individual zircon grains from the study area. Average continental crust evolution is modelled with $^{176}\text{Lu}/^{177}\text{Hf} = 0.0115$ (Condie, et al., 2005) and a mafic crust evolution with $^{176}\text{Lu}/^{177}\text{Hf} = 0.0210$ (Kramers, 2007). The two evolutionary trends proposed by different authors (Blichert-Toft & Puchtel, 2010; Griffin, et al., 2002) for the composition of the depleted mantle display similar results for Hafnium model ages, represented by stars at the intersection of depleted mantle and crustal evolution trends.

The evolution of magmatic suites in the NeoArchean terranes defines the following progression: (1) TTG magmatism, generated through the partial melting of mafic rocks; (2)

crust-derived biotite or two-mica granitic magmatism; (3) sanukitoids derived from a hybridized incompatible element-rich source and mantle peridotite, and (4) high-K hybrid granites displaying characteristics of the three previous suites (Feng & Kerrich, 1992; Laurent, et al., 2014; Smithies & Champion, 2000). Laurent, et al. (2014) contend that the distinct evolution and diversity of magmatism in Archean granitoids represents an ancient manifestation of subduction and tectonic collision. Despite the absence of sanukitoid-like rocks in the study area, the geochemical characteristics and pluton diversity together with emplacement sequenced recognised support a similar evolution is proposed for southern Ghana. Early subduction-related TTG magmatism from both the subducting slab and shallow partial melting of a basaltic source extracted from the depleted mantle between approximately ca. 2300 and 2260 Ma.

Coeval dioritic magmatism may be derived from the metasomatised mantle wedge and emplacement of minor hybrid, high-K plutons, followed by production of crust-derived peraluminous granites have a wider range of ϵHf values, consistent with continued contribution of radiogenic material from the depleted mantle at ~ 2250 Ma combined with recycled juvenile proto-crust with mantle extraction ages spanning from ~ 2650 to 2300 Ma. The latter suites are interpreted to highlight collision of continental fragments in the early Paleoproterozoic.

6.3 Implications for the crustal architecture of the West African Craton

A database compilation of Hf-isotope data for igneous and detrital zircons sourced from Paleoproterozoic rocks within the West African Craton is illustrated in Figure 5.14. Figure 5.14 contains all $\epsilon Hf_{(t)}$ values currently available for WAC (pale grey diamonds) (data sourced from: Block, *et al.*, 2016a; Eglinger, *et al.*, 2017; Parra-Avila, *et al.*, 2016; Petersson, *et al.*, 2017; Petersson, *et al.*, 2016), demonstrates the spectra of values within and between

discrete samples, highlights a 150 M.y. period of juvenile crust production between ~2250 and 2100 Ma, following a period of reworking of Archean crust for zircons aged between ca. 3200 and 2600 Ma. $\epsilon Hf(t)$ values for the Sefwi Belt (this study; Fig. 14) are consistently radiogenic, spanning from with +1 to +8, consistent with published ranges from the Palaeoproterozoic domain of the West African Craton.

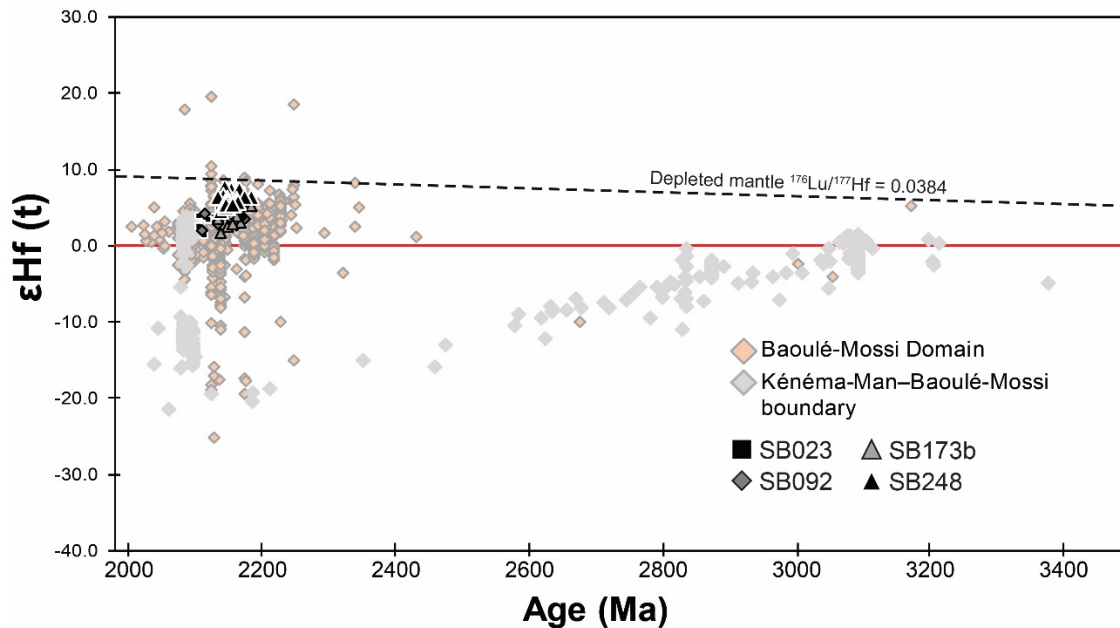


Fig. 14. Compilation of all $\epsilon Hf(t)$ values calculated for igneous and detrital zircons from within the Palaeoproterozoic Baoulé-Mossi domain (orange diamonds) and the boundary of the Archean Kénéman-Man and Baoulé-Mossi Domain (pale grey diamonds), relative to the evolution of the depleted mantle composition of (Griffin, et al., 2002), and values yielded by this study for igneous samples SB023, SB092, SB173B and SB248. Data sourced from Block, et al. (2016a), Eglinger, et al. (2017), Parra-Avila, et al. (2016) and Petersson, et al. (2016; 2017).

The radiogenic to strongly radiogenic Hf signatures preserved in the Sefwi Belt (this study; Petersson, et al., 2017) contrast the sub-chondritic Hf signatures of intrusions in the Kibi Belt in SE Ghana (Petersson, et al., 2017), as well as the more distal mixed Hf signatures near the

Archean-Paleoproterozoic boundary in southern Mali and Guinea (Eglinger, et al., 2017; Parra-Avila, et al., 2016), reflecting spatial variation in the isotopic record of the West African Craton. This data supports the conclusions of a number of authors who suggest that isotopic signatures of magmatic rocks in southern Ghana require a second, as yet unknown, Archean crustal source that lay southeast of the Baoulé-Mossi domain during crust formation (Petersson, et al., 2017; Taylor, et al., 1992). Further isotopic mapping of internal boundaries within the juvenile terranes of the WAC is somewhat limited by the capability of Hf analyses to recognise the reworking of recently created crust (Payne, *et al.*, 2016, and references therein), thus impeding our understanding of the crustal architecture through Hf-isotopes alone.

6.4 Conclusions: A geodynamic model for the southern West African Craton

Paleoproterozoic greenstone belts and granite-gneiss domains in the West African Craton have been likened to Archean provinces based on lithological and structural associations (e.g. Delor, et al., 1995; Lompo, 2009; Lompo, 2010; Vidal, et al., 1996; Vidal, et al., 2009), whilst others consider greenstone belts in West Africa as analogous to modern volcanic arcs (e.g. Baratoux, et al., 2011; Dampare, et al., 2008; Senyah, et al., 2016; Sylvester & Attoh, 1992). New geochemical and isotopic data presented in this study supports subduction-related magma generation, with most of the magmatic suites analysed from the Sefwi Greenstone Belt bearing geochemical signatures characteristic of arc environments. The proposed arc type environment is consistent with a growing body of evidence for volcanic arcs generated in a subduction setting within the West African Craton (Ama Salah, et al., 1996; Béziat, et al., 2000; Block, et al., 2016a; Lambert-Smith, *et al.*, 2016; Parra-Avila, et al., 2017; Petersson, et al., 2017; Petersson, et al., 2016; Sylvester & Attoh, 1992; Tapsoba, et al., 2013).

Accordingly, juvenile magmatism documented in the study area is likely sourced from both the metasomatised mantle wedge as well as the subducting slab. This suggests that the

geodynamic setting for crust production was hot enough to generate slab-derived melts, more than 250 Myrs after the proposed 2500 Ma end-date of slab derived melts (Martin, et al., 2009), reflecting a decrease in the Earth's heat production.

Whilst magmatism in the Sefwi Belt and the adjacent domain is consistent with the peak magmatic activity for the eastern block of the West African Craton (Parra-Avila, et al., 2017), there are multiple avenues of evidence which suggest southern Ghana docked onto central Ghana and the central east Ivory Coast at ca. 2090 Ma. Evidence includes collision-related crust-derived granitic magmatism along the north west margin of the Sefwi Belt between ca. 2092 and 2081 Ma (this study; Hirdes, et al., 1996; Hirdes, et al., 2007). This is complemented by documented clockwise P-T paths, peak HP-MT metamorphism and anatexis in paragneisses in the Chiraa Domain, and garnet amphibolites of the Kukuom-Juaboso Domain (McFarlane, 2018) with retrograde (post-peak T) metamorphism constrained by *in-situ* monazite U-Pb ages dated at ca. 2073 Ma (McFarlane, 2018). Within the broader context of the Paleoproterozoic Baoulé-Mossi Domain of the WAC, diachroneity in the geochronological record suggests additional crustal boundaries coincide the boundary located between the Banfora and Bagoé belts of western Burkina Faso and southern Mali, respectively, as identified by Parra-Avila, et al. (2017). Block, et al. (2016b) recently proposed a collisional event at ca. 2130 Ma between NW Ghana and western Burkina Faso/Ivory Coast associated with peak metamorphism and crustal anatexis, as well as contrasting tectonic histories. This coincides with peak magmatism and the first phase of the westward migration of magmatism from the eastern most portions of the Baoulé-Mossi domain to the central crustal boundary (Hirdes, et al., 1996; Parra-Avila, et al., 2017). Parra-Avila, et al. (2017) note a second westward migration of magmatism at ca. 2090 Ma, with subsequent synchronous subduction-related juvenile crust formation of the Kédougou-Kéniéma Inlier (Hirdes & Davis, 2002; Lambert-Smith, et al., 2016) and high-K magmatism

along the northern margin of the Kénéma Man Shield (Egal, et al., 2002; Eglinger, et al., 2017) during the docking of the Archean onto Paleoproterozoic domains. This protracted westward migration of magmatism and subsequent cessation of magmatism is incompatible with the timing of collision between the Kibi Belt and an Archean fragment at ca. 2140 Ma (Petersson, et al., 2017), and the subsequent collision along the NW margin of the Sefwi Belt between southern Ghana and central Ghana/eastern Ivory Coast between 2100 and 2080 Ma (this study). We, therefore, propose that the craton represents the ancient expression of a subduction-collision systems, with intermediate characteristics of late Archean and Phanerozoic accretionary orogenic systems, supporting the concept of the secular evolution and development of modern style plate tectonics during the Paleoproterozoic (Brown, 2006; Brown, 2007b).

The growing number of studies hypothesising collisions between smaller Paleoproterozoic terranes prior to their accretion to the Archean Kénéma-Man Domain suggests a complex accretionary-collisional history for the West African Craton. This raises important questions regarding the nascent Paleoproterozoic tectonic regime responsible for the formation and preservation of the craton. Do the tholeiitic basalts with oceanic plateau affinities and subsequent arc-related magmas of the WAC reflect the stagnant lid plate tectonic transition punctuated by bursts of subduction as hypothesised by Condie (2018)? Is there evidence of multiple, coeval subduction zones? Future work in the craton should ideally test these hypotheses, which will ultimately have significant implications for Paleoproterozoic subduction and orogen dynamics during this critical juncture in a transitional Earth.

8 Acknowledgements

We gratefully acknowledge AMIRA International and industry sponsors, including AusAid and the ARC Linkage Project LP110100667 for their support of the WAXI project (P934A), which funded the zircon SHRIMP analyses. Zircon analyses were carried out on the Sensitive High Resolution Ion Micro Probe mass spectrometer (SHRIMP II) at the John de Laeter Centre, Curtin University, with the financial support of the Australian Research Council and Auscope NCRIS. The contributions of Nicolas Thébaud were supported by the Hammond and Nisbet Fellowship at UWA. Field expenses were funded by the School of Earth, Atmosphere and Environment, Monash Research Initiative Fund – Dr L. Ailleres. Geochemical analyses were funded by the Institut de Recherche pour le Développement (IRD), provided by Dr. J. Ganne. We are deeply thankful to Chris Spencer for the zircon Lu-Hf analyses, which greatly improved and expanded our findings. We thank Massimo Raveggi, Rachelle Pierson and Junnel Alegado for their support in the sample preparation and mineral separation procedures. We thank Qing Qian and an anonymous reviewer for their detailed and constructive reviews that helped us greatly improve the manuscript. We also extend our gratitude to the Geological Survey Department of Ghana for their logistical support and data resources, as well as drivers from the GSD including Mr Kwasi Duah and Mr Brown.

9 References

- Abati, J., Aghzer, A. M., Gerdes, A. & Ennih, N., 2012. Insights on the crustal evolution of the West African Craton from Hf isotopes in detrital zircons from the Anti-Atlas belt. *Precambrian Research*, **212**, 263-274.
- Abouchami, W., Boher, M., Michard, A. & Albarede, F., 1990. A major 2.1 Ga event of mafic magmatism in West Africa: an early stage of crustal accretion. *Journal of Geophysical Research*, **95**(B11), 17,605-17,629.
- Adadey, K., Clarke, B., Théveniaut, H., Urien, P., Delor, C., Roig, J. Y. & Feybesse, J. L., 2009. Geological Map Explanation - Map Sheet 0503B (1:100 000), CGS/BRGM/Geoman. Geological Survey Department of Ghana (GSD).
- Ague, J., 2017. Element mobility during regional metamorphism in crustal and subduction zone environments with a focus on the rare earth elements (REE). *The American Mineralogist*, **102**(9), 1796-1821.
- Agyei Duodu, J., Loh, G. K., Boamah, K. O., Baba, M., Hirdes, W., Toloczyki, M. & Davis, D. W., 2009. Geological Map of Ghana 1:1 000 000, Geological Survey Department, Accra, Ghana.
- Albarède, F., 1998. The growth of continental crust. *Tectonophysics*, **296**(1), 1-14.

- Alderton, D. H. M., Pearce, J. A. & Potts, P. J., 1980. Rare earth element mobility during granite alteration: Evidence from southwest England. *Earth and Planetary Science Letters*, **49**(1), 149-165.
- Allibone, A., Teasdale, J., Cameron, G., Etheridge, M., Uttley, P., Soboh, A., Appiah-Kubi, J., Adanu, A., Arthur, R., Mamphey, J., Odoom, B., Zuta, J., Tsikata, A., Pataye, F., Famiyeh, S. & Lamb, E., 2002. Timing and structural controls on gold mineralization at the Bogoso Gold Mine, Ghana, West Africa. *Economic Geology*, **97**(5), 949-969.
- Ama Salah, I., Liegeois, J.-P. & Pouclet, A., 1996. Evolution d'un arc insulaire océanique birimien précoce au Liptako nigérien (Sirba): géologie, géochronologie et géochimie. *Journal of African Earth Sciences*, **22**(3), 235-254.
- Arculus, R., Lapierre, H. & Jaillard, E., 1999. Geochemical window into subduction and accretion processes: Raspas metamorphic complex, Ecuador. *Geology*, **27**(6), 547-550.
- Arndt, N., Albarede, F. & Nisbet, E., 1997. Mafic and ultramafic magmatism. *Oxford Monographs on geology and geophysics*, **35**(1), 233-254.
- Atherton, M. P. & Petford, N., 1993. Generation of sodium-rich magmas from newly underplated basaltic crust. *Nature*, **362**(6416), 144-146.
- Attoh, K. & Ekwueme, B., 1997. The West African Shield. *Oxford Monographs on Geology and Geophysics*, **35**(1), 517-528.
- Augustin, J. & Gaboury, D., 2017. Paleoproterozoic plume-related basaltic rocks in the Mana gold district in western Burkina Faso, West Africa: Implications for exploration and the source of gold in orogenic deposits. *Journal of African Earth Sciences*, **129**, 17-30.
- Baratoux, L., Metelka, V., Naba, S., Jessell, M. W., Grégoire, M. & Ganne, J., 2011. Juvenile Paleoproterozoic crust evolution during the Eburnean orogeny (~2.2 - 2 Ga), western Burkina Faso. *Precambrian Research*, **191**(1-2), 18-45.
- Barker, F., 1979. Trondhjemite: definition, environment and hypotheses of origin. In: *Trondhjemites, dacites and related rocks* (ed Barker, F.), pp. 1-12, Elsevier, Amsterdam.
- Bédard, J. H., 2006. A catalytic delamination-driven model for coupled genesis of Archaean crust and sub-continental lithospheric mantle. *Geochimica et Cosmochimica Acta*, **70**(5), 1188-1214.
- Belousova, E., Kostitsyn, Y., Griffin, W. L., Begg, G. C., O'Reilly, S. Y. & Pearson, N. J., 2010. The growth of the continental crust: constraints from zircon Hf-isotope data. *Lithos*, **119**(3), 457-466.
- Bessoles, B., 1977. Le Craton Ouest Africain. Géologie de l'Afrique Mémoires, BRGM, Paris, p. 88.
- Betts, P. G., Armit, R. J., Stewart, J., Aitken, A. R. A., Aillères, L., Donchak, P., Hutton, L., Withnall, I. & Giles, D., 2016. Australia and Nuna. *Geological Society, London, Special Publications*, **424**(1), 47-81.
- Béziat, D., Bourges, F., Debat, P., Lompo, M., Martin, F. & Tollon, F., 2000. A Paleoproterozoic ultramafic-mafic assemblage and associated volcanic rocks of the Boromo greenstone belt: fractionates originating from island-arc volcanic activity in the West African craton. *Precambrian Research*, **101**(1), 25-47.
- Blichert-Toft, J. & Puchtel, I. S., 2010. Depleted mantle sources through time: evidence from Lu-Hf and Sm-Nd isotope systematics of Archean komatiites. *Earth and Planetary Science Letters*, **297**(3), 598-606.
- Block, S., Baratoux, L., Zeh, A., Laurent, O., Bruguier, O., Jessell, M., Aillères, L., Sagna, R., Parra-Avila, L. A. & Bosch, D., 2016a. Paleoproterozoic juvenile crust formation and stabilisation in the south-eastern West African Craton (Ghana); New insights from U-Pb-Hf zircon data and geochemistry. *Precambrian Research*, **287**, 1-30.

- Block, S., Ganne, J., Baratoux, L., Zeh, A., Parra - Avila, L. A., Jessell, M., Aillères, L. & Siebenaller, L., 2015. Petrological and geochronological constraints on lower crust exhumation during Paleoproterozoic (Eburnean) orogeny, NW Ghana, West African Craton. *Journal of Metamorphic Geology*, **33**(5), 463-494.
- Block, S., Jessell, M., Aillères, L., Baratoux, L., Bruguier, O., Zeh, A., Bosch, D., Caby, R. & Mensah, E., 2016b. Lower crust exhumation during Paleoproterozoic (Eburnean) orogeny, NW Ghana, West African Craton: Interplay of coeval contractional deformation and extensional gravitational collapse. *Precambrian Research*, **274**, 82-109.
- Boher, M., Abouchami, W., Michard, A., Albarede, F. & Arndt, N. T., 1992. Crustal growth in West Africa at 2.1 Ga. *Journal of Geophysical Research: Solid Earth*, **97**(B1), 345-369.
- Bonhomme, M., 1962. Contribution à l'étude géochronologique de la plate-forme de l'Ouest Africain. *Annals de la Faculté des Sciences de Université de Clermont-Ferrand Géol. Minéral*, **5**, 62.
- Brown, G., Thorpe, R. & Webb, P., 1984. The geochemical characteristics of granitoids in contrasting arcs and comments on magma sources. *Journal of the Geological Society*, **141**(3), 413-426.
- Brown, M., 2006. Duality of thermal regimes is the distinctive characteristic of plate tectonics since the Neoproterozoic. *Geology*, **34**(11), 961-964.
- Brown, M., 2007a. Metamorphic Conditions in Orogenic Belts: A Record of Secular Change. *International Geology Review*, **49**(3), 193-234.
- Brown, M., 2007b. Metamorphism, Plate Tectonics, and the Supercontinent Cycle. *Earth Science Frontiers*, **14**(1), 1-18.
- Cagnard, F., Barbey, P. & Gapais, D., 2011. Transition between “Archean-type” and “modern-type” tectonics: Insights from the Finnish Lapland Granulite Belt. *Precambrian Research*, **187**(1), 127-142.
- Card, K., 1990. A review of the Superior Province of the Canadian Shield, a product of Archean accretion. *Precambrian Research*, **48**(1-2), 99-156.
- Cawood, P. A., Hawkesworth, C. J. & Dhuime, B., 2013. The continental record and the generation of continental crust. *GSA Bulletin*, **125**(1-2), 14-32.
- Cawood, P. A., Kröner, A., Collins, W. J., Kusky, T. M., Mooney, W. D. & Windley, B. F., 2009. Accretionary orogens through Earth history. *Geological Society, London, Special Publications*, **318**(1), 1-36.
- Chardon, D., Gapais, D. & Cagnard, F., 2009. Flow of ultra-hot orogens: A view from the Precambrian, clues for the Phanerozoic. *Tectonophysics*, **477**(3-4), 105-118.
- Clemens, J., 2003. S-type granitic magmas—petrogenetic issues, models and evidence. *Earth-Science Reviews*, **61**(1), 1-18.
- Clemens, J. & Vielzeuf, D., 1987. Constraints on melting and magma production in the crust. *Earth and Planetary Science Letters*, **86**(2), 287-306.
- Condie, K., 2015. Changing tectonic settings through time: Indiscriminate use of geochemical discriminant diagrams. *Precambrian Research*, **266**, 587-591.
- Condie, K. C., 1995. Episodic ages of Greenstones: A key to mantle dynamics? *Geophysical Research Letters*, **22**(16), 2215-2218.
- Condie, K. C., 1998. Episodic continental growth and supercontinents: a mantle avalanche connection? *Earth and Planetary Science Letters*, **163**(1), 97-108.
- Condie, K. C., 2008. Did the character of subduction change at the end of the Archean? Constraints from convergent-margin granitoids. *Geology*, **36**(8), 611-614.

- Condie, K. C., 2013. Preservation and recycling of crust during accretionary and collisional phases of Proterozoic orogens: A bumpy road from Nuna to Rodinia. *Geosciences*, **3**(2), 240-261.
- Condie, K. C., 2018. A planet in transition: The onset of plate tectonics on Earth between 3 and 2 Ga? *Geoscience Frontiers*, **9**(1), 51-60.
- Condie, K. C. & Aster, R. C., 2010. Episodic zircon age spectra of orogenic granitoids: The supercontinent connection and continental growth. *Precambrian Research*, **180**(3-4), 227-236.
- Condie, K. C. & Benn, K., 2006. Archean geodynamics: similar to or different from modern geodynamics? *Archean Geodynamics and Environments*, 47-59.
- Condie, K. C., Beyer, E., Belousova, E., Griffin, W. & O'Reilly, S. Y., 2005. U-Pb isotopic ages and Hf isotopic composition of single zircons: the search for juvenile Precambrian continental crust. *Precambrian Research*, **139**(1), 42-100.
- Condie, K. C., Bickford, M., Aster, R. C., Belousova, E. & Scholl, D. W., 2011. Episodic zircon ages, Hf isotopic composition, and the preservation rate of continental crust. *Geological Society of America Bulletin*, **123**(5-6), 951-957.
- Condie, K. C. & O'Neill, C., 2010. The Archean-Proterozoic boundary: 500 my of tectonic transition in Earth history. *American Journal of Science*, **310**(9), 775-790.
- Daigneault, R., Mueller, W. U. & Chown, E. H., 2002. Oblique Archean subduction: accretion and exhumation of an oceanic arc during dextral transpression, Southern Volcanic Zone, Abitibi Subprovince Canada. *Precambrian Research*, **115**(1-4), 261-290.
- Dampare, S. B., Shibata, T., Asiedu, D. K., Osae, S. & Banoeng-Yakubo, B., 2008. Geochemistry of Paleoproterozoic metavolcanic rocks from the southern Ashanti volcanic belt, Ghana: Petrogenetic and tectonic setting implications. *Precambrian Research*, **162**(3-4), 403-423.
- Davies, G. F., 2001. Dynamic Earth: Plates, plumes and mantle convection, AAPT.
- Davis, D. W., Hirdes, W., Schaltegger, U. & Nunoo, E. A., 1994. U-Pb age constraints on deposition and provenance of Birimian and gold-bearing Tarkwaian sediments in Ghana, West Africa. *Precambrian Research*, **67**(1-2), 89-107.
- de Kock, G. S., Armstrong, R. A., Siegfried, H. P. & Thomas, E., 2011. Geochronology of the Birim Supergroup of the West African craton in the Wa-Bolé region of west-central Ghana: Implications for the stratigraphic framework. *Journal of African Earth Sciences*, **59**(1), 1-40.
- de Kock, G. S., Théveniaut, H., Botha, P. M. W. & Gyapong, W., 2012. Timing the structural events in the Palaeoproterozoic Bolé-Nangodi belt terrane and adjacent Maluwe basin, West African craton, in central-west Ghana. *Journal of African Earth Sciences*, **65**(0), 1-24.
- de Wit, M. J., 1998. On Archean granites, greenstones, cratons and tectonics: does the evidence demand a verdict? *Precambrian Research*, **91**(1-2), 181-226.
- de Wit, M. J., de Ronde, C. E. J., Tredoux, M., Roering, C., Hart, R. J., Armstrong, R. A., Green, R. W. E., Peberdy, E. & Hart, R. A., 1992. Formation of an Archaean continent. *Nature*, **357**(6379), 553-562.
- Defant, M. J. & Drummond, M. S., 1990. Derivation of some modern arc magmas by melting of young subducted lithosphere. *Nature*, **347**(6294), 662-665.
- Defant, M. J. & Kepezhinskas, P., 2001. Evidence suggests slab melting in arc magmas. *Eos, Transactions American Geophysical Union*, **82**(6), 65-69.
- Delor, C., Siméon, Y. & Vidal, M., 1995. Peri-plutonic gravity driven deformations and transcurrent tectonics between 2.2 and 2.1 B.y.: A case study from the Birimian cycle in Ivory Coast. EUG 8 abstract. *Terra Nova*, **4**, 102.

- Dhuime, B., Hawkesworth, C. J., Cawood, P. A. & Storey, C. D., 2012. A change in the geodynamics of continental growth 3 billion years ago. *Science*, **335**(6074), 1334-1336.
- Doumbia, S., Pouclet, A., Kouamelan, A., Peucat, J. J., Vidal, M. & Delor, C., 1998. Petrogenesis of juvenile-type Birimian (Paleoproterozoic) granitoids in Central Côte-d'Ivoire, West Africa: geochemistry and geochronology. *Precambrian Research*, **87**, 33-63.
- Drummond, M., Defant, M. & Kepezhinskas, P., 1996. Petrogenesis of slab-derived trondhjemite-tonalite-dacite/adakite magmas. *Geological Society of America Special Papers*, **315**, 205-215.
- Drummond, M. S. & Defant, M. J., 1990. A model for trondhjemite - tonalite - dacite genesis and crustal growth via slab melting: Archean to modern comparisons. *Journal of Geophysical Research: Solid Earth*, **95**(B13), 21503-21521.
- Egal, E., Thiéblemont, D., Lahondère, D., Guerrot, C., Costea, C. A., Iliescu, D., Delor, C., Goujou, J.-C., Lafon, J. M., Tegye, M., Diaby, S. & Kolié, P., 2002. Late Eburnean granitization and tectonics along the western and northwestern margin of the Archean Kénéma-Man domain (Guinea, West African Craton). *Precambrian Research*, **117**(1-2), 57-84.
- Eglinger, A., Thébaud, N., Zeh, A., Davis, J., Miller, J., Parra-Avila, L. A., Loucks, R., McCuaig, C. & Belousova, E., 2017. New insights into the crustal growth of the Paleoproterozoic margin of the Archean Kéména-Man domain, West African craton (Guinea): Implications for gold mineral system. *Precambrian Research*, **292**, 258-289.
- Eisenlohr, B. N. & Hirdes, W., 1992. The structural development of the early Proterozoic Birimian and tarkwaian rocks of southwest Ghana, West Africa. *Journal of African Earth Sciences (and the Middle East)*, **14**(3), 313-325.
- Feng, R. & Kerrich, R., 1992. Geochemical evolution of granitoids from the Archean Abitibi Southern Volcanic Zone and the Pontiac subprovince, Superior Province, Canada: implications for tectonic history and source regions. *Chemical Geology*, **98**(1-2), 23-70.
- Feybesse, J.-L., Billa, M., Guerrot, C., Duguey, E., Lescuyer, J.-L., Milési, J.-P. & Bouchot, V., 2006. The Paleoproterozoic Ghanaian province: Geodynamic model and ore controls, including regional stress modeling. *Precambrian Research*, **149**(3 - 4), 149-196.
- Foley, S., Tiepolo, M. & Vannucci, R., 2002. Growth of early continental crust controlled by melting of amphibolite in subduction zones. *Nature*, **417**(6891), 837+.
- Galipp, K., Klemd, R. & Hirdes, W., 2003. Metamorphism and geochemistry of the Palaeoproterozoic Birimian Sefwi volcanic belt (Ghana, West Africa). *Geologisches Jahrbuch D 111*, 151 - 191.
- Ganne, J., De Andrade, V., Weinburg, R. F., Vidal, O., Dubacq, B., Kagambega, N., Naba, S., Baratoux, L., Jessell, M. W. & Allibone, J., 2012. Modern-style plate subduction preserved in the Palaeoproterozoic West African Craton. *Nature Geoscience Letters*, **5**, 60 - 65.
- Gasquet, D., Barbey, P., Adou, M. & Paquette, J. L., 2003. Structure, Sr-Nd isotope geochemistry and zircon U-Pb geochronology of the granitoids of the Dabakala area (Côte d'Ivoire): evidence for a 2.3 Ga crustal growth event in the Palaeoproterozoic of West Africa? *Precambrian Research*, **127**(4), 329-354.
- Goldfarb, R. J., André-Mayer, A.-S., Jowitt, S. M. & Mudd, G. M., 2017. West Africa: The World's Premier Paleoproterozoic Gold Province. *Economic Geology*, **112**(1), 123-143.

- Green, T., 1980. Island arc and continent-building magmatism—A review of petrogenic models based on experimental petrology and geochemistry. *Tectonophysics*, **63**(1-4), 367-385.
- Griffin, W., Wang, X., Jackson, S., Pearson, N., O'Reilly, S. Y., Xu, X. & Zhou, X., 2002. Zircon chemistry and magma mixing, SE China: in-situ analysis of Hf isotopes, Tonglu and Pingtan igneous complexes. *Lithos*, **61**(3), 237-269.
- Groves, D. I., Goldfarb, R. J., Gebre-Mariam, M., Hagemann, S. & Robert, F., 1998. Orogenic gold deposits: a proposed classification in the context of their crustal distribution and relationship to other gold deposit types. *Ore geology reviews*, **13**(1), 7-27.
- Gruau, G., Martin, H., Leveque, B., Capdevila, R. & Marot, A., 1985. Rb–Sr and Sm–Nd geochronology of lower Proterozoic granite–greenstone terrains in French Guiana, South America. *Precambrian Research*, **30**(1), 63-80.
- Gueye, M., Siegesmund, S., Wemmer, K., Pawlig, S., Drobe, M., Nolte, N. & Layer, P., 2007. New evidences for an early Birimian evolution in the West African Craton: An example from the Kédougou–Kéniéba inlier, southeast Senegal. *South African Journal of Geology*, **110**(4), 511-534.
- Halla, J., van Hunen, J., Heilimo, E. & Hölttä, P., 2009. Geochemical and numerical constraints on Neoproterozoic plate tectonics. *Precambrian Research*, **174**(1), 155-162.
- Hawkesworth, C., Cawood, P., Kemp, T., Storey, C. & Dhuime, B., 2009. Geochemistry: A matter of preservation. *Science*, **323**, 49-50.
- Hawkesworth, C., Dhuime, B., Pietranik, A., Cawood, P., Kemp, A. & Storey, C., 2010. The generation and evolution of the continental crust. *Journal of the Geological Society*, **167**(2), 229-248.
- Hawkesworth, C. & Kemp, A., 2006a. Evolution of the continental crust. *Nature*, **443**(7113), 811.
- Hawkesworth, C. & Kemp, A., 2006b. Using hafnium and oxygen isotopes in zircons to unravel the record of crustal evolution. *Chemical Geology*, **226**(3), 144-162.
- Hein, K. A. A., 2010. Succession of structural events in the Goren greenstone belt (Burkina Faso): Implications for West African tectonics. *Journal of African Earth Sciences*, **56**(2-3), 83-94.
- Herzberg, C., Condie, K. & Korenaga, J., 2010. Thermal history of the Earth and its petrological expression. *Earth and Planetary Science Letters*, **292**(1), 79-88.
- Hirdes, W. & Davis, D. W., 1998. First U–Pb zircon age of extrusive volcanism in the Birimian Supergroup of Ghana/West Africa. *Journal of African Earth Sciences*, **27**(2), 291-294.
- Hirdes, W. & Davis, D. W., 2002. U–Pb Geochronology of Paleoproterozoic Rocks in the Southern Part of the Kedougou–Kéniéba Inlier, Senegal, West Africa: Evidence for Diachronous Accretionary Development of the Eburnean Province. *Precambrian Research*, **118**(1-2), 83-99.
- Hirdes, W., Davis, D. W. & Eisenlohr, B. N., 1992. Reassessment of Proterozoic granitoid ages in Ghana on the basis of U/Pb zircon and monazite dating. *Precambrian Research*, **56**(1–2), 89-96.
- Hirdes, W., Davis, D. W., Lüdtke, G. & Konan, G., 1996. Two generations of Birimian (Paleoproterozoic) volcanic belts in northeastern Côte d'Ivoire (West Africa): consequences for the 'Birimian controversy'. *Precambrian Research*, **80**(3-4), 173-191.
- Hirdes, W., Konan, K. G., N'Da, D., Okou, A., Sea, P., Zamble, Z. B. & Davis, D. W., 2007. *Geology of the Northern Portion of the Oboisso Area, Côte d'Ivoire. Sheets 4A, 4B, 4B BIS, 4D.* Direction de la Géologie, Abidjan, Côte d'Ivoire and Bundesanstalt für Geowissenschaften und Rohstoffe, Hanover.

- Hirdes, W., Senger, R., Adjei, J., Efa, E., Loh, G. K. & Tettey, A., 1993. *Explanatory notes for the geological map of southwest Ghana 1:100 000*. Bundesanstalt für Geowissenschaften und Rohstoffe, Hannover.
- Hofmann, A., 1997. Mantle geochemistry: the message from oceanic volcanism. *Nature*, **385**(6613), 219-229.
- Irvine, T. & Baragar, W., 1971. A guide to the chemical classification of the common volcanic rocks. *Canadian journal of earth sciences*, **8**(5), 523-548.
- Jessell, M. W., Amponsah, P. O., Baratoux, L., Asiedu, D. K., Loh, G. K. & Ganne, J., 2012. Crustal-scale transcurrent shearing in the Paleoproterozoic Sefwi-Sunyani-Comoé region, West Africa. *Precambrian Research*, **212–213**(0), 155-168.
- John, T., Klemd, R., Hirdes, W. & Loh, G., 1999. The metamorphic evolution of the Paleoproterozoic (Birimian) volcanic Ashanti belt (Ghana, West Africa). *Precambrian Research*, **98**, 11-30.
- Junner, N. R., 1940. Geology of the Gold Coast and Western Togoland. *Gold Coast Geol. Surv. Bull.*, **11**(11), 1–40.
- Keller, C. B. & Schoene, B., 2012. Statistical geochemistry reveals disruption in secular lithospheric evolution about 2.5 Gyr ago. *Nature*, **485**(7399), 490.
- Klein, E. L., Moura, C. A. & Pinheiro, B. L., 2005. Paleoproterozoic crustal evolution of the São Luís Craton, Brazil: evidence from zircon geochronology and Sm-Nd isotopes. *Gondwana Research*, **8**(2), 177-186.
- Kramers, J. D., 2007. Hierarchical Earth accretion and the Hadean eon. *Journal of the Geological Society*, **164**(1), 3-17.
- Kuno, H., 1968. Differentiation of basalt magmas. In: *Basalts: The Poldervaart treatise on rocks of basaltic composition* (eds Hess, H. H. & Poldervaart, A.), pp. 623-688, Interscience, New York, N.Y.
- Lambert-Smith, J. S., Lawrence, D. M., Müller, W. & Treloar, P. J., 2016. Palaeotectonic setting of the south-eastern Kédougou-Kéniéba Inlier, West Africa: New insights from igneous trace element geochemistry and U-Pb zircon ages. *Precambrian Research*, **274**, 110–135.
- Large, R. R., Gemmill, J. B., Paulick, H. & Huston, D. L., 2001. The alteration box plot: A simple approach to understanding the relationship between alteration mineralogy and litho-geochemistry associated with volcanic-hosted massive sulfide deposits. *Economic geology*, **96**(5), 957-971.
- Laurent, O., Martin, H., Moyen, J.-F. & Doucelance, R., 2014. The diversity and evolution of late-Archean granitoids: Evidence for the onset of “modern-style” plate tectonics between 3.0 and 2.5 Ga. *Lithos*, **205**, 208-235.
- Le Maitre, R. W. B., Dudek, P., Keller, A., Lameyre, J., Le Bas, J., Sabine, M., Schmid, P., Sorensen, R., Streckeisen, H. & Woolley, A., 1989. *A classification of igneous rocks and glossary of terms: Recommendations of the International Union of Geological Sciences, Subcommittee on the Systematics of Igneous Rocks*. International Union of Geological Sciences.
- Leube, A., Hirdes, W., Mauer, R. & Kesse, G. O., 1990. The early Proterozoic Birimian Supergroup of Ghana and some aspects of its associated gold mineralization. *Precambrian Research*, **46**(1–2), 139-165.
- Lompo, M., 2009. Geodynamic evolution of the 2.25-2.0 Ga Palaeoproterozoic magmatic rocks in the Man-Leo shield of the West African Craton. A model of subsidence of an oceanic plateau. In: *Palaeoproterozoic Supercontinents and Global Evolution*, pp. 231-254, Geological Society, London.

- Lompo, M., 2010. Paleoproterozoic structural evolution of the Man-Leo Shield (West Africa). Key structures for vertical to transcurrent tectonics. *Journal of African Earth Sciences*, **58**, 19 - 36.
- Martin, H., 1986. Effect of steeper Archean geothermal gradient on geochemistry of subduction-zone magmas. *Geology*, **14**, 753-756.
- Martin, H., 1993. The mechanisms of petrogenesis of the Archean continental crust—comparison with modern processes. *Lithos*, **30**(3-4), 373-388.
- Martin, H. & Moyen, J.-F., 2002. Secular changes in tonalite-trondhjemite-granodiorite composition as markers of the progressive cooling of Earth. *Geology*, **30**(4), 319-322.
- Martin, H., Moyen, J.-F. & Rapp, R., 2009. The sanukitoid series: magmatism at the Archean–Proterozoic transition. *Earth and Environmental Science Transactions of the Royal Society of Edinburgh*, **100**(1-2), 15-33.
- Martin, H., Smithies, R. H., Rapp, R., Moyen, J. F. & Champion, D., 2005. An overview of adakite, tonalite–trondhjemite–granodiorite (TTG), and sanukitoid: relationships and some implications for crustal evolution. *Lithos*, **79**(1, 2), 1-24.
- McDonough, W., Sun, S.-S., Ringwood, A., Jagoutz, E. & Hofmann, A., 1992. Potassium, rubidium, and cesium in the Earth and Moon and the evolution of the mantle of the Earth. *Geochimica et Cosmochimica Acta*, **56**(3), 1001-1012.
- McDonough, W. F. & Sun, S.-S., 1995. The composition of the Earth. *Chemical geology*, **120**(3), 223-253.
- McFarlane, H. B., 2018. *The geodynamic and tectonic evolution of the Palaeoproterozoic Sefwi Greenstone Belt, West African Craton (Ph.D. Manuscript)*, Monash University.
- McFarlane, H. B., Ailleres, L., Betts, P., Ganne, J., Baratoux, L., Jessell, M. W. & Block, S., 2019. Episodic collisional orogenesis and lower crust exhumation during the Palaeoproterozoic Eburnean Orogeny: Evidence from the Sefwi Greenstone Belt, West African Craton. *Precambrian Research*, **325**, 88-110.
- Milési, J. P., Feybesse, J. L., Pinna, P., Deschamps, Y., Kampunzu, H., Muhongo, S., Lescuyer, J.-L., Le Goff, E., Delor, C., Billa, M., Ralay, F. & Henry, C., 2004. Geological map of Africa 1: 10,000,000, SIGAfrique project. In: *20th Conference of African Geology, BRGM*, <http://www.sigafrique.net>, Orléans, France, 2-7 June.
- Milési, J. P., Ledru, P., Feybesse, J.-L., Dommaget, A. & Marcoux, E., 1992. Early Proterozoic ore deposits and tectonics of the Birimian orogenic belt, West Africa. *Precambrian Research*, **58**, 305 - 344.
- Moyen, J.-F., 2009. High Sr/Y and La/Yb ratios: the meaning of the “adakitic signature”. *Lithos*, **112**(3), 556-574.
- Moyen, J.-F., 2011. The composite Archean grey gneisses: petrological significance, and evidence for a non-unique tectonic setting for Archean crustal growth. *Lithos*, **123**(1), 21-36.
- Moyen, J.-F. & Martin, H., 2012. Forty years of TTG research. *Lithos*, **148**, 312-336.
- Moyen, J.-F. & Stevens, G., 2006a. Experimental Constraints on TTG Petrogenesis: Implications for Archean Geodynamics. In: *Archean Geodynamics and Environments*, pp. 149-175, American Geophysical Union.
- Moyen, J. F. & Stevens, G., 2006b. Experimental constraints on TTG petrogenesis: implications for Archean geodynamics. *Archean geodynamics and environments*, 149-175.
- Nance, R. D., Worsley, T. R. & Moody, J. B., 1988. The supercontinent cycle. *Scientific American*, **259**(1), 72-79.
- O'Connor, J., 1965. A classification for quartz-rich igneous rocks based on feldspar ratios. *US Geological Survey Professional Paper B*, **525**, 79-84.

- Oberthür, T., Vetter, U., Davis, D. W. & Amanor, J. A., 1998. Age constraints on gold mineralization and Paleoproterozoic crustal evolution in the Ashanti belt of southern Ghana. *Precambrian Research*, **89**(3-4), 129-143.
- Parra-Avila, L., 2015. 4D Evolution of the Paleoproterozoic Baoulé-Mossi Domain of the West African Craton. *Unpublished Ph. D thesis. University of Western Australia*, 527.
- Parra-Avila, L. A., Belousova, E., Fiorentini, M. L., Baratoux, L., Davis, J., Miller, J. & McCuaig, T. C., 2016. Crustal evolution of the Paleoproterozoic Birimian terranes of the Baoulé-Mossi domain, southern West African Craton: U–Pb and Hf-isotope studies of detrital zircons. *Precambrian Research*, **274**, 25-60.
- Parra-Avila, L. A., Kemp, A. I. S., Fiorentini, M. L., Belousova, E., Baratoux, L., Block, S., Jessell, M., Bruguier, O., Begg, G. C., Miller, J., Davis, J. & McCuaig, T. C., 2017. The geochronological evolution of the Paleoproterozoic Baoulé-Mossi domain of the Southern West African Craton. *Precambrian Research*, **300**, 1-27.
- Patchett, P. J., Vervoort, J. D., Söderlund, U. & Salters, V. J. M., 2004. Lu–Hf and Sm–Nd isotopic systematics in chondrites and their constraints on the Lu–Hf properties of the Earth. *Earth and Planetary Science Letters*, **222**(1), 29-41.
- Pawlig, S., Gueye, M., Klischies, R., Schwarz, S., Wemmer, K. & Siegesmund, S., 2006. Geochemical and Sr-Nd isotopic data on the Birimian of the Kedougou-Kenieba inlier (Eastern Senegal): Implications on the Palaeoproterozoic evolution of the West African craton. *South African Journal of Geology*, **109**(3), 411-427.
- Payne, J. L., McInerney, D. J., Barovich, K. M., Kirkland, C. L., Pearson, N. J. & Hand, M., 2016. Strengths and limitations of zircon Lu-Hf and O isotopes in modelling crustal growth. *Lithos*, **248**, 175-192.
- Pearce, J. A., Harris, N. B. & Tindle, A. G., 1984. Trace element discrimination diagrams for the tectonic interpretation of granitic rocks. *Journal of petrology*, **25**(4), 956-983.
- Percival, J. A., Stern, R. A., Skulski, T., Card, K. D., Mortensen, J. K. & Begin, N. J., 1994. Minto block, Superior province: Missing link in deciphering assembly of the craton at 2.7 Ga. *Geology*, **22**(9), 839-842.
- Perrouty, S., Aillères, L., Jessell, M. W., Baratoux, L., Bourassa, Y. & Crawford, B., 2012. Revised Eburnean geodynamic evolution of the gold-rich southern Ashanti Belt, Ghana, with new field and geophysical evidence of pre-Tarkwaian deformations. *Precambrian Research*, **204–205**, 12-39.
- Petersson, A., Scherstén, A. & Gerdes, A., 2017. Extensive reworking of Archaean crust within the Birimian terrane in Ghana as revealed by combined zircon U-Pb and Lu-Hf isotopes. *Geoscience Frontiers*.
- Petersson, A., Scherstén, A., Kemp, A., Kristinsdóttir, B., Kalvig, P. & Anum, S., 2016. Zircon U-Pb-Hf evidence for subduction related crustal growth and reworking of Archaean crust within the Palaeoproterozoic Birimian terrane, West African Craton, SE Ghana. *Precambrian Research*, **275**, 286-309.
- Peucat, J.-J., Capdevila, R., Drareni, A., Mahdjoub, Y. & Kahoui, M., 2005. The Eglab massif in the West African Craton (Algeria), an original segment of the Eburnean orogenic belt: petrology, geochemistry and geochronology. *Precambrian Research*, **136**(3-4), 309-352.
- Pigois, J. P., Groves, D. I., Fletcher, I. R., McNaughton, N. J. & Snee, L. W., 2003. Age constraints on Tarkwaian palaeoplacer and lode-gold formation in the Tarkwa-Damang district, SW Ghana. *Mineralium Deposita*, **38**(6), 695-714.
- Potrel, A., Peucat, J. J. & Fanning, C. M., 1998. Archean crustal evolution of the West African Craton: example of the Amsaga Area (Reguibat Rise): U-Pb and Sm-Nd evidence for crustal growth and recycling. *Precambrian Research*, **90**(3–4), 107-117.

- Poucllet, A., Doumbia, S. & Vidal, M., 2006. Geodynamic setting of the Birimian volcanism in central Ivory Coast (western Africa) and its place in the Palaeoproterozoic evolution of the Man Shield. *Bulletin de la Societe Geologique de France*, **177**(2), 105-121.
- Poujol, M., Robb, L. J., Anhaeusser, C. R. & Gericke, B., 2003. A review of the geochronological constraints on the evolution of the Kaapvaal Craton, South Africa. *Precambrian Research*, **127**(1), 181-213.
- Puetz, S. J., Condie, K. C., Pisarevsky, S., Davaille, A., Schwarz, C. J. & Ganade, C. E., 2017. Quantifying the evolution of the continental and oceanic crust. *Earth-Science Reviews*, **164**, 63-83.
- Puetz, S. J., Ganade, C. E., Zimmermann, U. & Borchardt, G., 2018. Statistical analyses of global U-Pb database 2017. *Geoscience Frontiers*, **9**(1), 121-145.
- Qian, Q. & Hermann, J., 2013. Partial melting of lower crust at 10–15 kbar: constraints on adakite and TTG formation. *Contributions to Mineralogy and Petrology*, **165**(6), 1195-1224.
- Rapp, R., Shimizu, N., Norman, M. & Applegate, G., 1999. Reaction between slab-derived melts and peridotite in the mantle wedge: experimental constraints at 3.8 GPa. *Chemical Geology*, **160**(4), 335-356.
- Rapp, R. P. & Watson, E. B., 1995. Dehydration melting of metabasalt at 8–32 kbar: implications for continental growth and crust-mantle recycling. *Journal of Petrology*, **36**(4), 891-931.
- Rapp, R. P., Watson, E. B. & Miller, C. F., 1991. Partial melting of amphibolite/eclogite and the origin of Archean trondhjemites and tonalites. *Precambrian Research*, **51**(1–4), 1-25.
- Rey, P. F. & Houseman, G., 2006. Lithospheric scale gravitational flow: the impact of body forces on orogenic processes from Archaean to Phanerozoic. *Geological Society, London, Special Publications*, **253**(1), 153-167.
- Rogers, J. J. & Santosh, M., 2004. *Continents and supercontinents*. Oxford University Press.
- Rogers, J. J. W. & Santosh, M., 2002. Configuration of Columbia, a Mesoproterozoic Supercontinent. *Gondwana Research*, **5**(1), 5-22.
- Rollinson, H., 2016. Archaean crustal evolution in West Africa: A new synthesis of the Archaean geology in Sierra Leone, Liberia, Guinea and Ivory Coast. *Precambrian Research*, **281**, 1-12.
- Rudnick, R. & Gao, S., 2003. Composition of the continental crust. *Treatise on geochemistry*, **3**, 1-64.
- Senyah, G. A., Dampare, S. B. & Asiedu, D. K., 2016. Geochemistry and tectonic setting of the Paleoproterozoic metavolcanic rocks from the Chirano Gold District, Sefwi belt, Ghana. *Journal of African Earth Sciences*, **122**, 32-46.
- Shirey, S. B. & Hanson, G. N., 1984. Mantle-derived Archaean monozodiorites and trachyandesites. *Nature*, **310**(5974), 222-224.
- Siegfried, P., De Kock, G., Clarke, B., Agenbacht, A., Delor, C. & Van Rooyen, R., 2009. Geological map explanation–map sheet 0903D (1: 100 000). *Mining Sector Support Programme. CGS, BRGM, Geoman, GSD, Accra*.
- Sizova, E., Gerya, T., Brown, M. & Perchuk, L., 2010. Subduction styles in the Precambrian: insight from numerical experiments. *Lithos*, **116**(3), 209-229.
- Smithies, R., 2000. The Archaean tonalite–trondhjemite–granodiorite (TTG) series is not an analogue of Cenozoic adakite. *Earth and Planetary Science Letters*, **182**(1), 115-125.
- Smithies, R. & Champion, D., 2000. The Archaean high-Mg diorite suite: links to tonalite–trondhjemite–granodiorite magmatism and implications for early Archaean crustal growth. *Journal of Petrology*, **41**(12), 1653-1671.

- Smithies, R., Van Kranendonk, M. & Champion, D., 2005. It started with a plume—early Archaean basaltic proto-continental crust. *Earth and Planetary Science Letters*, **238**(3), 284-297.
- Sorjonen-Ward, P. & Luukkonen, E., 2005. Archean rocks. *Developments in Precambrian Geology*, **14**, 19-99.
- Soumaila, A., Henry, P., Garba, Z. & Rossi, M., 2008. REE patterns, Nd-Sm and U-Pb ages of the metamorphic rocks of the Diagorou-Darbani greenstone belt (Liptako, SW Niger): implication for Birimian (Palaeoproterozoic) crustal genesis. *Geological Society, London, Special Publications*, **297**(1), 19-32.
- Spencer, C. J., Murphy, J. B., Kirkland, C. L., Liu, Y. & Mitchell, R. N., 2018. A Palaeoproterozoic tectono-magmatic lull as a potential trigger for the supercontinent cycle. *Nature Geoscience*, **11**(2), 97-101.
- Stern, R. A., Hanson, G. N. & Shirey, S. B., 1989. Petrogenesis of mantle-derived, LILE-enriched Archean monzodiorites and trachyandesites (sanukitoids) in southwestern Superior Province. *Canadian Journal of Earth Sciences*, **26**(9), 1688-1712.
- Sylvester, P. J. & Attoh, K., 1992. Lithostratigraphy and Composition of 2.1 Ga Greenstone Belts of the West African Craton and Their Bearing on Crustal Evolution and the Archean-Proterozoic Boundary. *The Journal of Geology*, **100**(4), 377-393.
- Tapsoba, B., Lo, C.-H., Jahn, B.-M., Chung, S.-L., Wenmenga, U. & Iizuka, Y., 2013. Chemical and Sr–Nd isotopic compositions and zircon U–Pb ages of the Birimian granitoids from NE Burkina Faso, West African Craton: Implications on the geodynamic setting and crustal evolution. *Precambrian Research*, **224**, 364-396.
- Taylor, P. N., Moorbath, S., Leube, A. & Hirdes, W., 1992. Early Proterozoic crustal evolution in the birimian of Ghana: constraints from geochronology and isotope geochemistry. *Precambrian Research*, **56**(1–2), 97-111.
- Taylor, S. R. & McLennan, S. M., 1985. The continental crust: its composition and evolution.
- Théveniaut, H., Delor, C., Lafon, J., Monié, P., Rossi, P. & Lahondère, D., 2006. Paleoproterozoic (2155–1970Ma) evolution of the Guiana Shield (Transamazonian event) in the light of new paleomagnetic data from French Guiana. *Precambrian Research*, **150**(3), 221-256.
- Tshibubudze, A., Hein, K., Peters, L., Woolfe, A. & McCUAIG, T., 2013. Oldest U-Pb crystallization age for the West African Craton from the Oudalan-Gorouol Belt of Burkina Faso. *South African Journal of Geology*, **116**(1), 169-181.
- Tshibubudze, A., Hein, K. A. A. & Marquis, P., 2009. The Markoye Shear Zone in NE Burkina Faso. *Journal of African Earth Sciences*, **55**(5), 245-256.
- Vidal, M. & Alric, G., 1994. The palaeoproterozoic (Birimian) of Haute-Comoé in the West African craton, Ivory Coast: a transtensional back-arc basin. *Precambrian Research*, **65**(1–4), 207-229.
- Vidal, M., Delor, C., Pouclet, A., Simeon, Y. & Alric, G., 1996. Geodynamic evolution of West Africa between 2.2 and 2 Ga: the Archean style of the Birimian greenstone belts and the sedimentary basins in northeastern Ivory Coast. *Bulletin de la Societe Geologique de France*, **167**(3), 307-319.
- Vidal, M., Gumiaux, C., Cagnard, F., Pouclet, A., Ouattara, G. & Pichon, M., 2009. Evolution of a Paleoproterozoic "weak type" orogeny in the West African Craton (Ivory Coast). *Tectonophysics*, **477**(3-4), 145-159.
- Wang, Q., Wyman, D. A., Xu, J.-F., Zhao, Z.-H., Jian, P., Xiong, X.-L., Bao, Z.-W., Li, C.-F. & Bai, Z.-H., 2006. Petrogenesis of Cretaceous adakitic and shoshonitic igneous rocks in the Luzong area, Anhui Province (eastern China): implications for geodynamics and Cu–Au mineralization. *Lithos*, **89**(3), 424-446.
- Windley, B. F., 1984. The Archaean-Proterozoic boundary. *Tectonophysics*, **105**(1-4), 43-53.

- Woodhead, J., Eggins, S. & Gamble, J., 1993. High field strength and transition element systematics in island arc and back-arc basin basalts: evidence for multi-phase melt extraction and a depleted mantle wedge. *Earth and Planetary Science Letters*, **114**(4), 491-504.
- Xiong, X., Adam, J. & Green, T., 2005. Rutile stability and rutile/melt HFSE partitioning during partial melting of hydrous basalt: implications for TTG genesis. *Chemical Geology*, **218**(3), 339-359.
- Zeh, A., Gerdes, A. & Barton, J. M., 2009. Archean accretion and crustal evolution of the Kalahari Craton—the zircon age and Hf isotope record of granitic rocks from Barberton/Swaziland to the Francistown Arc. *Journal of Petrology*, **50**(5), 933-966.
- Zeh, A., Jaguin, J., Poujol, M., Boulvais, P., Block, S. & Paquette, J.-L., 2013. Juvenile crust formation in the northeastern Kaapvaal Craton at 2.97 Ga—Implications for Archean terrane accretion, and the source of the Pietersburg gold. *Precambrian Research*, **233**, 20-43.
- Zhao, G., Cawood, P. A., Wilde, S. A. & Sun, M., 2002. Review of global 2.1–1.8 Ga orogens: implications for a pre-Rodinia supercontinent. *Earth-Science Reviews*, **59**(1–4), 125-162.
- Zitzmann, A., Keissling, R. & Loh, G. K., 1997. *Geological, geophysical and geochemical investigations in the Bui Belt area in Ghana*. Geologische Jahrbuch, Reihe B, Hannover; Accra.

Onset of the supercontinent cycle: evidence for multiple oceanic arc accretion events in the Sefwi Greenstone Belt of the West African Craton

McFarlane, H. B.^{1,2,3}, Thébaud, N.³, Parra-Avilla, L.A.^{3,4}, Armit, R.¹, Spencer, C.⁵, Ganne, J.², Aillères, L.¹, Baratoux, L.^{2,6}, Betts, P. G.¹, and Jessell, M. W.^{2,3}

Highlights:

- New petrological, geochemical and isotopic study of the understudied Palaeoproterozoic Sefwi Greenstone Belt, SW Ghana, in the West African Craton;
- Subduction-related arc magmatism derived from the mantle wedge and partial melting of the subducting slab, followed by crust-derived granitic magmatism;
- Radiogenic $\varepsilon Hf_{(t)}$ values ranging from +1.6 to +7.6 for felsic magmatic units, indicating radiogenic input and an older crustal component (>2650 Ma);
- Juvenile crust formation and preservation attributed to possibly earliest subduction-related accretionary-collisional orogen of the Palaeoproterozoic during transition to modern plate tectonic regime.